Ecole des Mines

October-November 2014

Cosserat Point Elements (CPEs) for nonlinear elasticity

MB Rubin* and M Jabareen**

*Faculty of Mechanical Engineering
Technion - Israel Institute of Technology
32000 Haifa, Israel
Email: mbrubin@tx.technion.ac.il

** Faculty of Civil and Environmental Engineering
Technion - Israel Institute of Technology
32000 Haifa, Israel
Email: cvjmah@techunix.technion.ac.il

1. Introduction

A nonlinear hyperelastic elastic material has one of the simplest constitutive equations because the stress response is determined algebraically by derivatives of a strain energy function. However, the nonlinear partial differential equations which describe the deformation of an elastic material are intractable analytically for most problems. Therefore, numerical methods are essential to obtain solutions of realistic problems.

Examination of the commercial programs ABAQUS, ADINA, ANSYS and the academic code FEAP reveals that the user has to choose from a list of different hyperlastic elements (see Table 1.1). This list includes element formulations based on full integration (Q1), full integration of distortion and reduced integration of volume (Q1P0), reduced integration with various types of hourglass controls, hybrid methods, incompatible modes and enhanced strains. The reason for this extensive list is that no single element performs well for all element geometries, levels of compressibility and under all loading conditions. In particular, it is well known that, within the context of the Bubnov-Galerkin approach based on a tri-linear approximation of the displacement field, full integration of the constitutive equations leads to an element response which exhibits locking for bending dominated response of thin structures (shells and rods) with poor element aspect ratios and for nearly incompressible materials. Two main modifications of the element formulations have been proposed to overcome these problems. One modification uses reduced integration with hourglass control (e.g. Belytschko et al., 1984; Hutter et al., 2000; Reese and Wriggers, 1996; Reese et al., 2000) and the second modification uses enhanced strains or incompatible modes (e.g. Simo and Armero, 1992;

Simo and Rifai, 1990; Simo et al., 1993). Moreover, the enhanced strain and incompatible mode elements exhibit hourglass instabilities in regions of high compression combined with bending (e.g. Reese and Wriggers, 1996; Reese et al., 2000; Jabareen and Rubin, 2007a,b).

Short Name	Program	Element Name	Options
ABAQUS-1	ABAQUS	C3D8(S)	full integration ($\bar{B}$ method)
ABAQUS-2	ABAQUS	C3D8R(S)	reduced integration hourglass control: enhanced
ABAQUS-3	ABAQUS	C3D8R(S)	reduced integration hourglass control: stiffness
ABAQUS-4	ABAQUS	C3D8RH(S)	hybrid formulation reduced integration hourglass control: enhanced
ABAQUS-5	ABAQUS	C3D8RH(S)	hybrid formulation reduced integration hourglass control: stiffness
ABAQUS-6	ABAQUS	C3D8I(S)	incompatible modes
ABAQUS-7	ABAQUS	C3D8IH(S)	hybrid formulation incompatible modes
ADINA-1	ADINA	3D Solid (8 Nodes)	full integration
ADINA-2	ADINA	3D Solid (8 Nodes)	incompatible modes
ANSYS-1	ANSYS	Solid185	pure displacement with full integration
ANSYS-2	ANSYS	Solid185	pure displacement with reduced integration and hourglass control
ANSYS-3	ANSYS	Solid185	pure displacement with enhanced strain
ANSYS-4	ANSYS	Solid185	pure displacement with simplified enhanced strain
ANSYS-5	ANSYS	Hyper86	full integration
ANSYS-6	ANSYS	Hyper86	full integration for shear and reduced integration for volume
FEAP-1	FEAP	Solid-Fini-Disp-8	full integration
FEAP-2	FEAP	Solid-Fini-Mixe-8	mixed formulation
FEAP-3	FEAP	Solid-Fini-Enha-8	enhanced strain

Table 1.1 List of elements tested in the programs ABAQUS, ADINA, ANSYS and FEAP.

Often the person who wants to solve a specific problem using a hyperelastic constitutive equations typically does not know which of the element formulations in the code is best suited for the specific problem. Sometimes a problem can be sufficiently

complicated that none of these elements can provide accurate predictions for the deformation fields in all regions of the problem. In this sense the existing element formulations are not user friendly.

Therefore, there appears to be a need for a robust user friendly element formulation that can be reliably used for all applications. The 3-D brick Cosserat Point Element (CPE) is a new element technology that is based on the theory of a Cosserat point (Rubin, 1985a,b; 1995; 2000) and which has been proven (Nadler and Rubin, 2003; Jabareen and Rubin, 2007a,b,c,e) to be such a robust user friendly element for nonlinear elasticity. In particular, it does not exhibit unphysical locking or hourglassing for thin structures or nearly incompressible material response.

2. Basic tensor operations

Before developing the equations for a CPE it is useful to review some tensor operations. Basic knowledge of index notation and simple vector operations is assumed and more details of tensor operations can be found in (Rubin, 2000).

Tensor product

Let $\{\mathbf{a}_i, \mathbf{b}_i\}$ (i=1,2,3,4) be sets of vectors in three-dimensional space. Then, the tensor product is denoted by the symbol $\otimes$ and the tensor product $\mathbf{a}_1 \otimes \mathbf{a}_2$ of two vectors is defined by its operation on another vector $\mathbf{b}_1$, such that

$$(\mathbf{a}_1 \otimes \mathbf{a}_2)\, \mathbf{b}_1 = \mathbf{a}_1\, (\mathbf{a}_2 \bullet \mathbf{b}_1) = (\mathbf{a}_2 \bullet \mathbf{b}_1)\, \mathbf{a}_1 \ , \ \mathbf{b}_1\, (\mathbf{a}_1 \otimes \mathbf{a}_2) = (\mathbf{b}_1 \bullet \mathbf{a}_1)\, \mathbf{a}_2 \ , \qquad (2.1)$$

where $(\mathbf{a}_2 \bullet \mathbf{b}_1)$ denotes the scalar product between the two vectors $\{\mathbf{a}_2, \mathbf{b}_1\}$. A scalar is called a zero order tensor and a vector is called a first order tensor. The quantity $(\mathbf{a}_1 \otimes \mathbf{a}_2)$ is called a second order tensor because it is linear operator which maps the space of vectors onto a tensor of one order lower than itself (i.e. a first order tensor). That is to say that the result of $(\mathbf{a}_1 \otimes \mathbf{a}_2)$ operating on a vector is a vector. In general, the result when $\mathbf{b}_1$ is placed to the right of $(\mathbf{a}_1 \otimes \mathbf{a}_2)$ is different than when it is placed to the left of $(\mathbf{a}_1 \otimes \mathbf{a}_2)$.

The tensor product can be used to create higher order tensors by creating a string of vectors, separated by tensor products. For example, the quantity $(\mathbf{a}_1 \otimes \mathbf{a}_2 \otimes \mathbf{a}_3 \otimes \mathbf{a}_4)$ is a fourth order tensor which satisfies the conditions

$$(\mathbf{a}_1 \otimes \mathbf{a}_2 \otimes \mathbf{a}_3 \otimes \mathbf{a}_4)\, \mathbf{b}_1 = (\mathbf{a}_4 \bullet \mathbf{b}_1)\, (\mathbf{a}_1 \otimes \mathbf{a}_2 \otimes \mathbf{a}_3) \ ,$$

$$\mathbf{b}_1\, (\mathbf{a}_1 \otimes \mathbf{a}_2 \otimes \mathbf{a}_3 \otimes \mathbf{a}_4) = (\mathbf{b}_1 \bullet \mathbf{a}_1)\, (\mathbf{a}_2 \otimes \mathbf{a}_3 \otimes \mathbf{a}_4) \ . \qquad (2.2)$$

Juxtaposition of two tensors

The operation of juxtaposition is used when two tensor are placed next to each other. For example

$$(\mathbf{a}_1\otimes\mathbf{a}_2)(\mathbf{b}_1\otimes\mathbf{b}_2) = \mathbf{a}_1\otimes(\mathbf{a}_2 \bullet \mathbf{b}_1)\mathbf{b}_2 = (\mathbf{a}_2 \bullet \mathbf{b}_1)(\mathbf{a}_1\otimes\mathbf{b}_2) \ , \tag{2.3a}$$

$$(\mathbf{b}_1\otimes\mathbf{b}_2)(\mathbf{a}_1\otimes\mathbf{a}_2) = (\mathbf{b}_2 \bullet \mathbf{a}_1)\ (\mathbf{b}_1\otimes\mathbf{a}_2) \neq (\mathbf{a}_1\otimes\mathbf{a}_2)(\mathbf{b}_1\otimes\mathbf{b}_2) \ . \tag{2.3b}$$

In particular, note that the operation of juxtaposition is not commutative so that the two tensors in (2.3a,b) are not necessarily equal. Moreover, it is noted that the operation of juxtaposition involves the scalar product of only one vector from each of the tensors. It will be shown later that this operation yields results that are the same as standard multiplication of matrices.

Dot product of two tensors

The scalar product or dot product of two vectors is a positive definite operator which is defined so that the dot product of a vector with itself is positive as long as the vector is nonzero. The dot product of two tensors is also defined as a positive definite operator. Specifically, it is defined so that

$$(\mathbf{a}_1\otimes\mathbf{a}_2) \bullet (\mathbf{b}_1\otimes\mathbf{b}_2) = (\mathbf{a}_1 \bullet \mathbf{b}_1)(\mathbf{a}_2 \bullet \mathbf{b}_2) = (\mathbf{b}_1\otimes\mathbf{b}_2) \bullet (\mathbf{a}_1\otimes\mathbf{a}_2) \ ,$$

$$(\mathbf{a}_1\otimes\mathbf{a}_2\otimes\mathbf{a}_3\otimes\mathbf{a}_4) \bullet (\mathbf{b}_1\otimes\mathbf{b}_2) = (\mathbf{a}_3 \bullet \mathbf{b}_1)(\mathbf{a}_4 \bullet \mathbf{b}_2)\ (\mathbf{a}_1\otimes\mathbf{a}_2) \ ,$$

$$(\mathbf{b}_1\otimes\mathbf{b}_2) \bullet (\mathbf{a}_1\otimes\mathbf{a}_2\otimes\mathbf{a}_3\otimes\mathbf{a}_4) = (\mathbf{b}_1 \bullet \mathbf{a}_1)(\mathbf{b}_2 \bullet \mathbf{a}_2)(\mathbf{a}_3\otimes\mathbf{a}_4) \neq (\mathbf{a}_1\otimes\mathbf{a}_2\otimes\mathbf{a}_3\otimes\mathbf{a}_4) \bullet (\mathbf{b}_1\otimes\mathbf{b}_2) \ ,$$

$$(\mathbf{a}_1\otimes\mathbf{a}_2\otimes\mathbf{a}_3\otimes\mathbf{a}_4) \bullet (\mathbf{b}_1\otimes\mathbf{b}_2\otimes\mathbf{b}_3\otimes\mathbf{b}_4) = (\mathbf{a}_1 \bullet \mathbf{b}_1)(\mathbf{a}_2 \bullet \mathbf{b}_2)(\mathbf{a}_3 \bullet \mathbf{b}_3)(\mathbf{a}_4 \bullet \mathbf{b}_4) \ . \tag{2.4}$$

In particular, note that the dot product of two tensors has the order of the difference of the orders of the tensors (e.g. the dot product of two tensors of the same order is a scalar and

the dot product of a tensor of fourth order with a tensor of second order is a tensor of second order).

Transpose of a tensor

The transpose of a tensor is obtained by interchanging the order of the vectors associated with the order of the transpose operator. For example, the right transpose (denoted by a superposed T) and the left transpose (denoted by a superposed LT) are defined so that

$$(\mathbf{a}_1\otimes\mathbf{a}_2)^{T} = (\mathbf{a}_2\otimes\mathbf{a}_1) \ , \ {}^{RT}(\mathbf{a}_1\otimes\mathbf{a}_2) = (\mathbf{a}_2\otimes\mathbf{a}_1) \ ,$$

$$(\mathbf{a}_1\otimes\mathbf{a}_2\otimes\mathbf{a}_3\otimes\mathbf{a}_4)^{T} = (\mathbf{a}_1\otimes\mathbf{a}_2)\otimes(\mathbf{a}_4\otimes\mathbf{a}_2) \ , \ {}^{RT}(\mathbf{a}_1\otimes\mathbf{a}_2\otimes\mathbf{a}_3\otimes\mathbf{a}_4) = (\mathbf{a}_2\otimes\mathbf{a}_1)\otimes(\mathbf{a}_3\otimes\mathbf{a}_4) \ . \quad (2.5)$$

Notice that the operators T and RT change the order of the two vectors closest to the operator.

It is also possible to define higher order transpose operations like T(2) and RT(2) which apply to pairs of two vectors, such that

$$(\mathbf{a}_1\otimes\mathbf{a}_2\otimes\mathbf{a}_3\otimes\mathbf{a}_4)^{T(2)} = (\mathbf{a}_3\otimes\mathbf{a}_4)\otimes(\mathbf{a}_1\otimes\mathbf{a}_2) = {}^{RT(2)}(\mathbf{a}_1\otimes\mathbf{a}_2\otimes\mathbf{a}_3\otimes\mathbf{a}_4) \ . \quad (2.6)$$

General tensors

Although the tensor $(\mathbf{a}_1\otimes\mathbf{a}_2)$ is a second order tensor it is not a general second order tensor. In order to discuss general tensors it is convenient to first consider tensors referred to a rectangular Cartesian triad $\mathbf{e}_i$ (i=1,2,3) of constant orthonormal vectors

$$\mathbf{e}_i \bullet \mathbf{e}_j = \delta_{ij} \ , \quad (2.7)$$

where δ_{ij} denotes the Kroneker delta

$$\delta_{ij} = 1 \ \text{ for } i=j \quad \text{and} \quad \delta_{ij} = 0 \ \text{ for } i\neq j \ . \quad (2.8)$$

It is well known that the vectors $\mathbf{e}_i$ form a complete set of base vectors that span the space of three-dimensional vectors so that an arbitrary vector $\mathbf{v}$ can be expressed in terms of its components v_i relative to $\mathbf{e}_i$, such that

$$v_i = \mathbf{v} \bullet \mathbf{e}_i \ , \ \mathbf{v} = v_i \, \mathbf{e}_i \ , \tag{2.9}$$

where the usual summation convention is used over repeated indices, which take the values (i=1,2,3). In a similar manner it is possible to define a set of nine orthonormal base tensors $(\mathbf{e}_i \otimes \mathbf{e}_j)$ that span the space of second order tensors with

$$(\mathbf{e}_i \otimes \mathbf{e}_j) \bullet (\mathbf{e}_m \otimes \mathbf{e}_n) = \delta_{im} \, \delta_{jn} \ . \tag{2.10}$$

Then, an arbitrary second order tensor $\mathbf{T}$ can be expressed in terms of its components T_{ij} relative to $\mathbf{e}_i$, such that

$$T_{ij} = \mathbf{T} \bullet (\mathbf{e}_i \otimes \mathbf{e}_j) \ , \quad \mathbf{T} = T_{ij} \, (\mathbf{e}_i \otimes \mathbf{e}_j) \ . \tag{2.11}$$

Also, an arbitrary fourth order tensor $\mathbf{T}$ can be expressed in terms of its components T_{ijmn} relative to $\mathbf{e}_i$, such that

$$T_{ijmn} = \mathbf{T} \bullet (\mathbf{e}_i \otimes \mathbf{e}_j \otimes \mathbf{e}_m \otimes \mathbf{e}_n) \ , \quad \mathbf{T} = T_{ijmn} \, (\mathbf{e}_i \otimes \mathbf{e}_j \otimes \mathbf{e}_m \otimes \mathbf{e}_n) \ . \tag{2.12}$$

In particular, it is noted that a general second order tensor has $3^2=9$ independent components and a general fourth order tensor has $3^4=81$ independent components.

Representation of tensors with respect to curvilinear coordinates

Within the context of the CPE theory it is convenient to express some tensors using the same symbol as is typically used in the three-dimensional theory. Thus, in order to distinguish between these quantities a superposed (*) is used for the three-dimensional quantity. For example, the position vector of a material point in the deformed present configuration associated with the three-dimensional theory is denoted by $\mathbf{x}^*$ instead of $\mathbf{x}$.

The rectangular Cartesian base vectors $\mathbf{e}_i$ are special in that they are constants which are independent of the coordinates x_i^*. Consequently, the position vector $\mathbf{x}^*$ can be expressed in the form

$$\mathbf{x}^* = x_i^* \, \mathbf{e}_i \ , \tag{2.13}$$

so that the base vectors $\mathbf{e}_i$ can be determined by the equations

$$\mathbf{e}_i = \frac{\partial \mathbf{x}^*}{\partial x_i^*} \ . \tag{2.14}$$

For general curvilinear coordinates the position vector $\mathbf{x}^*$ is a function of three convected coordinates θ^i (i=1,2,3) and time t, such that

$$\mathbf{x}^* = \mathbf{x}^*(\theta^i, t) \ . \tag{2.15}$$

The convected coordinates θ^i have constant values for a specified material point and the need for distinguishing between subscripts and superscripts will become apparent. The covariant base vectors $\mathbf{g}_i$ defined by

$$\mathbf{g}_i = \mathbf{x}^*{}_{,i} = \frac{\partial \mathbf{x}^*}{\partial \theta^i} \ , \tag{2.16}$$

are generalizations of the base vectors $\mathbf{e}_i$ in (2.14). Here, and throughout the text, a comma is used to denote partial differentiation with respect to the coordinates θ^i. Also, it is noted that the mapping (2.15) is limited so that it is one-to-one with $\mathbf{g}_i$ being linearly independent vectors

$$g^{1/2} = \mathbf{g}_1 \times \mathbf{g}_2 \bullet \mathbf{g}_3 > 0 \ , \tag{2.17}$$

that span the three-dimensional space. The main difference between $\mathbf{g}_i$ and $\mathbf{e}_i$ is that $\mathbf{g}_i$ can depend on the coordinates θ^i. This has an important influence on expressions related

to the gradient and divergence operators. Moreover, since θ^i do not necessarily have the units of length (i.e. the angle in cylindrical polar coordinates), $\mathbf{g}_i$ need not be unitless.

Since $\mathbf{g}_i$ are linearly independent it is possible to define reciprocal vectors $\mathbf{g}^i$ (also called contravariant base vectors) by the expressions

$$\mathbf{g}^1 = g^{-1/2}\, \mathbf{g}_2 \times \mathbf{g}_3 \ , \ \mathbf{g}^2 = g^{-1/2}\, \mathbf{g}_3 \times \mathbf{g}_1 \ , \ \mathbf{g}^3 = g^{-1/2}\, \mathbf{g}_1 \times \mathbf{g}_2 \ , \tag{2.18}$$

such that

$$\mathbf{g}^i \bullet \mathbf{g}_j = \delta^i_{\ j} \ , \tag{2.19}$$

where $\delta^i_{\ j}$ is the Kroneckor delta symbol. Now, an arbitrary vector $\mathbf{v}$ can be expressed in terms of its covariant components v_i or its contravariant components v^i

$$v_i = \mathbf{v} \bullet \mathbf{g}_i \ , \ v^i = \mathbf{v} \bullet \mathbf{g}^i \ , \ \mathbf{v} = v_i\, \mathbf{g}^i = v^i\, \mathbf{g}_i \ . \tag{2.20}$$

Similarly, an arbitrary second order tensor $\mathbf{T}$ can be expressed in terms of its covariant components T_{ij}, its contravariant components T^{ij}, or its mixed components $\{T^i_{\ j}, T_i^{\ j}\}$

$$T_{ij} = \mathbf{T} \bullet (\mathbf{g}_i \otimes \mathbf{g}_j) \ , \ T^{ij} = \mathbf{T} \bullet (\mathbf{g}^i \otimes \mathbf{g}^j) \ , \ T^i_{\ j} = \mathbf{T} \bullet (\mathbf{g}^i \otimes \mathbf{g}_j) \ , \ T_i^{\ j} = \mathbf{T} \bullet (\mathbf{g}_i \otimes \mathbf{g}^j) \ ,$$

$$\mathbf{T} = T_{ij}\, (\mathbf{g}^i \otimes \mathbf{g}^j) = T^{ij}\, (\mathbf{g}_i \otimes \mathbf{g}_j) = T^i_{\ j}\, (\mathbf{g}_i \otimes \mathbf{g}^j) = T_i^{\ j}\, (\mathbf{g}^i \otimes \mathbf{g}_j) \ . \tag{2.21}$$

In particular, notice that the summation connects covariant components with contravariant base vectors or contravariant components with covariant base vectors. Furthermore, it can be shown that the unit second order tensor $\mathbf{I}$ can be expressed in the forms

$$\mathbf{I} = \mathbf{g}_i \otimes \mathbf{g}^i = \mathbf{g}^i \otimes \mathbf{g}_i \ . \tag{2.22}$$

Referential description

In continuum mechanics it is sometimes convenient to introduce a stress-free reference configuration. Specifically, the material point in the reference configuration that is associated with the position $\mathbf{x}^*$ in the present configuration is denoted by $\mathbf{X}^*$

$$\mathbf{X}^* = \mathbf{X}^*(\theta^i) \ , \tag{2.23}$$

and is independent of time t. It then follows that the associated covariant base vectors $\mathbf{G}_i$, and contravariant base vectors $\mathbf{G}^i$ are defined by expressions similar to (2.16)-(2.19)

$$\mathbf{G}_i = \mathbf{X}^*_{,i} \ , \ G^{1/2} = \mathbf{G}_1 \times \mathbf{G}_2 \bullet \mathbf{G}_3 \ , \ \mathbf{G}^i \bullet \mathbf{G}_j = \delta^i_j \ ,$$

$$\mathbf{G}^1 = G^{-1/2}\, \mathbf{G}_2 \times \mathbf{G}_3 \ , \ \mathbf{G}^2 = G^{-1/2}\, \mathbf{G}_3 \times \mathbf{G}_1 \ , \ \mathbf{G}^3 = G^{-1/2}\, \mathbf{G}_1 \times \mathbf{G}_2 \ . \tag{2.24}$$

Also, the unit tensor $\mathbf{I}$ can be written in the alternative forms

$$\mathbf{I} = \mathbf{G}_i \otimes \mathbf{G}^i = \mathbf{G}^i \otimes \mathbf{G}_i \ . \tag{2.25}$$

Gradient operator

The gradient of a tensor $\mathbf{T}$ relative to the reference position $\mathbf{X}^*$ is denoted by $\mathrm{Grad}^*\mathbf{T}$ and the gradient of $\mathbf{T}$ relative to the present position $\mathbf{x}^*$ is denoted by $\mathrm{grad}^*\mathbf{T}$, which are defined by

$$\mathrm{Grad}^*\mathbf{T} = \partial \mathbf{T}/\partial \mathbf{X}^* = \mathbf{T}_{,i} \otimes \mathbf{G}^i \ , \ \mathrm{grad}^*\mathbf{T} = \partial \mathbf{T}/\partial \mathbf{x}^* = \mathbf{T}_{,i} \otimes \mathbf{g}^i \ . \tag{2.26}$$

Divergence operator

The divergence of a tensor $\mathbf{T}$ relative to the reference position $\mathbf{X}^*$ is denoted by $\mathrm{Div}^*\mathbf{T}$ and the divergence of $\mathbf{T}$ relative to the present position $\mathbf{x}^*$ is denoted by $\mathrm{div}^*\mathbf{T}$, which are defined by

$$\mathrm{Div}^*\mathbf{T} = \mathbf{T}_{,i} \bullet \mathbf{G}^i \ , \ \mathrm{div}^*\mathbf{T} = \mathbf{T}_{,i} \bullet \mathbf{g}^i \ . \tag{2.27}$$

The divergence operators can be simplified by differentiating (2.17), (2.18) and (2.24) to prove the identity

$$(G^{1/2}\,\mathbf{G}^i)_{,i} = 0 \;\;, (g^{1/2}\,\mathbf{g}^i)_{,i} = 0 \;\;, \tag{2.28}$$

Then, $\mathrm{Div}^*\mathbf{T}$ and $\mathrm{div}^*\mathbf{T}$ can be expressed in the alternative forms

$$\mathrm{Div}^*\mathbf{T} = G^{-1/2}\,(G^{1/2}\,\mathbf{T}\,\mathbf{G}^i)_{,i} \;\;,\;\; \mathrm{div}^*\mathbf{T} = g^{-1/2}\,(g^{1/2}\,\mathbf{T}\,\mathbf{g}^i)_{,i} \;\;. \tag{2.29}$$

This form is simpler than (2.27) because the derivative of **T** includes derivatives of the components of **T** as well as derivatives of each of the base vectors. For example, if **T** is a second order tensor then

$$\mathbf{T}_{,i} = [T_{mn}\,(\mathbf{g}^m \otimes \mathbf{g}^n)]_{,i} = T_{mn,i}\,(\mathbf{g}^m \otimes \mathbf{g}^n) + T_{mn}\,(\mathbf{g}^m{}_{,i} \otimes \mathbf{g}^n) + T_{mn}\,(\mathbf{g}^m \otimes \mathbf{g}^n{}_{,i}) \;, \tag{2.30}$$

whereas, the expressions in (2.29) is based on derivatives of vectors.

3. Some kinematic measures in continuum mechanics

In continuum mechanics the material point $\mathbf{X}^*$ in the fixed reference configuration it mapped to the location $\mathbf{x}^*$ in the deformed present configuration by the expression (2.15). The absolute velocity $\mathbf{v}^*$ of the material point is obtained by

$$\mathbf{v}^* = \dot{\mathbf{x}}^* = \frac{\partial \mathbf{x}^*(\theta^i,t)}{\partial t} \ , \tag{3.1}$$

where the material time derivative is denoted by a superposed dot (•) which indicates partial differentiation with respect to time t holding the convected coordinates θ^i constants.

The deformation gradient $\mathbf{F}^*$ is a two-point tensor that maps material line element $d\mathbf{X}^*$ in the reference configuration to material line elements $d\mathbf{x}^*$ in the present configuration

$$d\mathbf{x}^* = \mathbf{F}^* d\mathbf{X}^* \ , \quad \mathbf{F}^* = \partial \mathbf{x}^* / \partial \mathbf{X}^* = \mathrm{Grad}^* \mathbf{x}^* \ . \tag{3.2}$$

Using the results in Section 2 it can be shown that $\mathbf{F}^*$ can be expressed in terms of the base vectors by

$$\mathbf{F}^* = \mathbf{g}_i \otimes \mathbf{G}^i \ . \tag{3.3}$$

Moreover, the dilatation J^*

$$J^* = \det(\mathbf{F}^*) = \frac{g^{1/2}}{G^{1/2}} = \frac{dv^*}{dV^*} \ , \tag{3.4}$$

is a pure measure of volume change since the element of volume dV^* in the reference configuration and the element of volume dv^* in the present configuration are given by

$$dV^* = G^{1/2} d\theta^1 d\theta^2 d\theta^3 \ , \ dv^* = g^{1/2} d\theta^1 d\theta^2 d\theta^3 \ . \tag{3.5}$$

Next, taking the material derivative of $\mathbf{F}^*$ and using the fact that $\mathbf{G}^i$ are independent of time it can be shown that

$$\dot{\mathbf{F}}^* = \dot{\mathbf{g}}_i \otimes \mathbf{G}^i = \mathbf{v}^*{}_{,i} \otimes \mathbf{G}^i = \mathbf{L}^* \mathbf{g}_i \otimes \mathbf{G}^i = \mathbf{L}^* \mathbf{F}^* \quad , \tag{3.6}$$

where $\mathbf{L}^*$ is the velocity gradient

$$\mathbf{L}^* = \partial \mathbf{v}^* / \partial \mathbf{x}^* = \mathbf{v}^*{}_{,j} \otimes \mathbf{g}^j \quad . \tag{3.7}$$

The velocity gradient $\mathbf{L}^*$ separates into its symmetric part $\mathbf{D}^*$, called the rate of deformation tensor and its skew-symmetric part $\mathbf{W}^*$, called the spin tensor, such that

$$\mathbf{L}^* = \mathbf{D}^* + \mathbf{W}^* \quad , \quad \mathbf{D}^* = \frac{1}{2}(\mathbf{L}^* + \mathbf{L}^{*\mathrm{T}}) = \mathbf{D}^{*\mathrm{T}} \quad , \quad \mathbf{W}^* = \frac{1}{2}(\mathbf{L}^* - \mathbf{L}^{*\mathrm{T}}) = -\mathbf{W}^{*\mathrm{T}} \quad . \tag{3.8}$$

Moreover, it can be shown that the material derivative of the dilatation J^* is given by

$$\dot{J}^* = J^* \, \mathbf{D}^* \bullet \mathbf{I} \quad . \tag{3.9}$$

4. Balance laws in curvilinear coordinates

Let P denote the current material region of space occupied by a body and let ∂P be its smooth closed boundary. Also, let P_0 be the material region occupied by the same body in its fixed reference configuration with ∂P_0 being its smooth closed boundary. Then, the balance laws of the purely mechanical theory can be expressed as the conservation of mass

$$\int_P \rho^* \, dv^* = \int_{P_0} \rho_0^* \, dV^* \ , \tag{4.1}$$

the balance of linear momentum

$$\frac{d}{dt}\int_P \rho^* \mathbf{v}^* \, dv^* = \int_P \rho^* \mathbf{b}^* \, dv^* + \int_{\partial P} \mathbf{t}^* \, da^* \ , \tag{4.2}$$

and the balance of angular momentum about the fixed origin

$$\frac{d}{dt}\int_P \mathbf{x}^* \times \rho^* \mathbf{v}^* \, dv^* = \int_P \mathbf{x}^* \times \rho^* \mathbf{b}^* \, dv^* + \int_{\partial P} \mathbf{x}^* \times \mathbf{t}^* \, da^* \ . \tag{4.3}$$

In these expressions, ρ^* is the current mass density, ρ_0^* is its reference value, $\mathbf{b}^*$ is the body force per unit mass, $\mathbf{t}^*$ is the surface traction and da^* is the element of area in the present configuration. Also, it is recalled that the traction vector is related to the Cauchy stress tensor $\mathbf{T}^*$ and the unit outward normal vector $\mathbf{n}^*$ to ∂P^* by the expression

$$\mathbf{t}^* = \mathbf{T}^* \, \mathbf{n}^* \ . \tag{4.4}$$

Next, using (3.5) and the divergence theorem in the form

$$\int_P \mathrm{div}^* \mathbf{A} \, dv^* = \int_{\partial P} \mathbf{A} \, \mathbf{n}^* \, da^* \ , \tag{4.5}$$

the local forms of the conservation of mass and the balance of linear momentum become

$$m^* = \rho^* g^{1/2} = \rho_0^* \, G^{1/2} = m^*(\theta^i) \ , \quad m^* \dot{\mathbf{v}}^* = m^* \mathbf{b}^* + \mathbf{t}^{*j}{}_{,j} \ , \tag{4.6a,b}$$

where use has been made of (2.28) and the three vectors $\mathbf{t}^{*i}$ are defined by

$$\mathbf{t}^{*i} = g^{1/2}\mathbf{T}^*\mathbf{g}^i \ . \tag{4.7}$$

Also, using the balance laws (4.6) the reduced form of the balance of angular momentum requires the Cauchy stress tensor to be symmetric

$$\mathbf{T}^{*T} = \mathbf{T}^* \ . \tag{4.8}$$

Within the context of the purely mechanical theory it is convenient to define the rate of work $\mathcal{W}$ done on the body, the kinetic energy $\mathcal{K}$ and the strain energy $\mathcal{U}$ of the body by the expressions

$$\mathcal{W} = \int_P \rho^*\mathbf{b}^* \bullet \mathbf{v}^* \, dv^* + \int_{\partial P} \mathbf{t}^* \bullet \mathbf{v}^* \, da^* ,$$

$$\mathcal{K} = \int_P \frac{1}{2}\rho^*\mathbf{b}^* \bullet \mathbf{v}^* \, dv^* \ , \quad \mathcal{U} = \int_P \rho^*\Sigma^* \, dv^* \ , \tag{4.9}$$

where Σ^* is the strain energy function per unit mass. Then, the rate of material dissipation $\mathcal{D}^*$ per unit present volume can be defined by

$$\int_P \mathcal{D}^* \, dv^* = \mathcal{W} - \dot{\mathcal{K}} - \dot{\mathcal{U}} \geq 0 \ , \tag{4.10}$$

and is required to be non-negative. Next, using the balance laws (4.6) and (4.8) it can be shown that

$$\mathcal{D}^* = \mathbf{T}^* \bullet \mathbf{D}^* - \rho^*\dot{\Sigma}^* \geq 0 \ . \tag{4.11}$$

For a nonlinear elastic solid the strain energy depends on the deformation gradient $\mathbf{F}^*$ through the deformation tensor $\mathbf{C}^*$

$$\Sigma^* = \Sigma^*(\mathbf{C}^*) \ , \ \mathbf{C}^* = \mathbf{F}^*\mathbf{F}^{*T} \ , \tag{4.12}$$

the stress $\mathbf{T}^*$ is assumed to be independent of deformation rate and the rate of dissipation $\mathscr{D}^*$ vanishes. These assumptions lead to the result that the stress is given by the hyperelastic constitutive equation

$$\mathbf{T}^* = 2\rho^* \mathbf{F}^* \frac{\partial \Sigma^*}{\partial \mathbf{C}^*} \mathbf{F}^{*\mathrm{T}} \ . \tag{4.13}$$

Using the work of Flory (1961) it is possible to separate the effects of dilation from distortion. Specifically, the dilation J^* defined by

$$J^* = \det(\mathbf{F}^*) \ , \tag{4.14}$$

is a pure measure of volume change and the symmetric, unimodular tensor $\mathbf{B}^{*\prime}$ defined by

$$\mathbf{B}^{*\prime} = J^{*-2/3} \mathbf{B}^* \ , \ \mathbf{B}^* = \mathbf{F}^* \mathbf{F}^{*\mathrm{T}} \ , \ \det(\mathbf{B}^{*\prime}) = 1 \ , \tag{4.15}$$

is a pure measure of distortional deformation. It therefore, follows that $\mathbf{B}^{*\prime}$ has only two nontrivial invariants, which can be defined by

$$\alpha_1^* = \mathbf{B}^{*\prime} \bullet \mathbf{I} \ , \quad \alpha_2^* = \mathbf{B}^{*\prime} \bullet \mathbf{B}^{*\prime} \ . \tag{4.16}$$

Thus, for an elastically isotropic material the strain energy function Σ^* can be expressed in the form

$$\Sigma^* = \Sigma^*(J^*, \alpha_1^*, \alpha_2^*) \ . \tag{4.17}$$

Moreover, in the examples considered here, attention is focused on the special case of a compressible Neo-Hookean material defined by

$$\rho_0^* \Sigma^* = \frac{1}{2} K (J^*-1)^2 + \frac{1}{2} \mu (\alpha_1^* - 3) \ , \tag{4.18}$$

where $\{K, \mu\}$ are the small deformation bulk and shear modulus, respectively, and Poisson's ratio ν is defined such that

$$K = \frac{2\mu(1+\nu)}{3(1-2\nu)} \ . \tag{4.19}$$

Unless otherwise stated, for the example problems considered in the later sections the material is taken to be compressible with the strain energy function (4.18) and with the material constants specified by

$$K = 1 \text{ GPa} \ , \ \mu = 0.6 \text{ GPa} \ , \ \nu = 0.25 \ . \tag{4.20}$$

For the special examples which consider a nearly incompressible the material constants are specified by

$$K = 1000 \text{ GPa} \ , \ \mu = 0.6 \text{ GPa} \ , \ \nu \approx 0.4997 \ . \tag{4.21}$$

5. Bubnov-Galerkin equations for a 3-D brick element

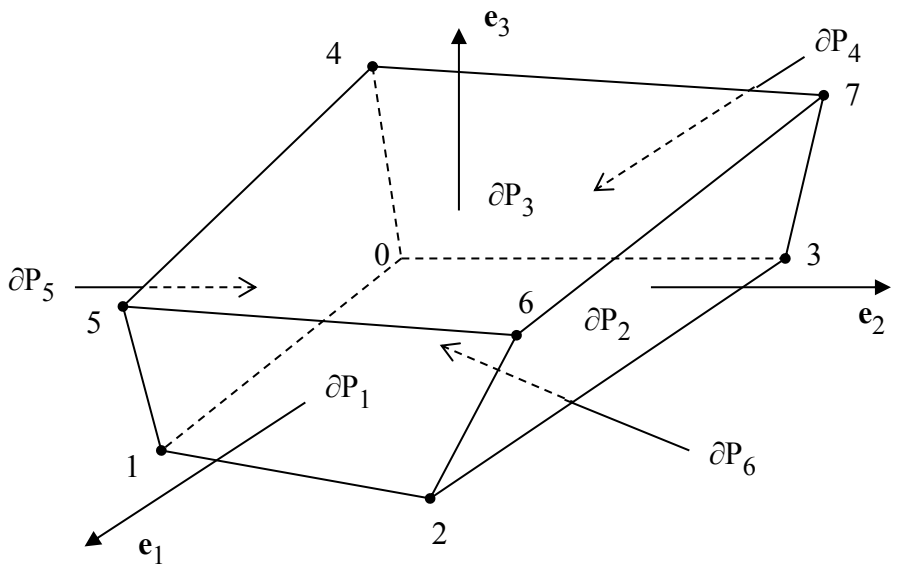

Fig. 5.1 Sketch of a general brick CPE showing the numbering of the nodes and the surfaces.

Figure 5.1 shows a sketch of a 3-D brick element which occupies the region P with closed boundary ∂P characterized by the union of the six surfaces ∂P_I (I=1,2,…,6). Within the context of the Bubnov-Galerkin approach based on tri-linear shape functions, the position vector $\mathbf{X}^*$ of a material point in the reference configuration is represented by

$$\mathbf{X}^* = \mathbf{X}^*(\theta^i) = \sum_{m=0}^{7} N^m(\theta^i)\, \mathbf{D}_m \ , \tag{5.1}$$

where the shape functions $N^m(\theta^i)$ depend only on the convected coordinates θ^i and are given by

$$N^0 = 1 \ , \ N^1 = \theta^1 \ , \ N^2 = \theta^2 \ , \ N^3 = \theta^3 \ ,$$

$$N^4 = \theta^1\theta^2 \ , \ N^5 = \theta^1\theta^3 \ , \ N^6 = \theta^2\theta^3 \ , \ N^7 = \theta^1\theta^2\theta^3 \ , \tag{5.2}$$

and the reference element director vectors $\mathbf{D}_i$ (i=0,1,…,7) are constant vectors with $\mathbf{D}_i$ (i=1,2,3) being linearly independent

$$D^{1/2} = \mathbf{D}_1 \times \mathbf{D}_2 \bullet \mathbf{D}_3 > 0 \ . \tag{5.3}$$

The locations of the nodes in the reference configuration are characterized by the constant reference nodal director vectors $\bar{\mathbf{D}}_i$ (i=0,1,…,7). In particular, the convected coordinates are limited by the lengths H_i (i=1,2,3), such that

$$|\theta^1| \le \frac{H_1}{2} \ , \ |\theta^2| \le \frac{H_2}{2} \ , |\theta^3| \le \frac{H_3}{2} \ , \tag{5.4}$$

and that

$$\bar{\mathbf{D}}_0 = \mathbf{X}^*(-\frac{H_1}{2}, -\frac{H_2}{2}, -\frac{H_3}{2}) \ , \ \bar{\mathbf{D}}_1 = \mathbf{X}^*(\frac{H_1}{2}, -\frac{H_2}{2}, -\frac{H_3}{2}) \ ,$$

$$\bar{\mathbf{D}}_2 = \mathbf{X}^*(\frac{H_1}{2}, \frac{H_2}{2}, -\frac{H_3}{2}) \ , \ \bar{\mathbf{D}}_3 = \mathbf{X}^*(-\frac{H_1}{2}, \frac{H_2}{2}, -\frac{H_3}{2}) \ ,$$

$$\bar{\mathbf{D}}_4 = \mathbf{X}^*(-\frac{H_1}{2}, -\frac{H_2}{2}, \frac{H_3}{2}) \ , \ \bar{\mathbf{D}}_5 = \mathbf{X}^*(\frac{H_1}{2}, -\frac{H_2}{2}, \frac{H_3}{2}) \ ,$$

$$\bar{\mathbf{D}}_6 = \mathbf{X}^*(\frac{H_1}{2}, \frac{H_2}{2}, \frac{H_3}{2}) \ , \ \bar{\mathbf{D}}_7 = \mathbf{X}^*(-\frac{H_1}{2}, \frac{H_2}{2}, \frac{H_3}{2}) \ . \tag{5.5}$$

Also, the lengths H_i are defined so that $\mathbf{D}_i$ (i=1,2,3) are unit vectors

$$|\mathbf{D}_1| = |\mathbf{D}_2| = |\mathbf{D}_3| = 1 \ . \tag{5.6}$$

In the Bubnov-Galerkin approach it is also assumed that the position vector $\mathbf{x}^*$ of material points in the present configuration can be expressed using a representation of the form (5.1) with the reference element directors $\mathbf{D}_i$ replaced by the present element directors $\mathbf{d}_i(t)$, which are functions of time t only, such that

$$\mathbf{x}^* = \mathbf{x}^*(\theta^i,t) = \sum_{m=0}^{7} N^m(\theta^i)\, \mathbf{d}_m(t) \ , \tag{5.7}$$

where it is assumed that $\mathbf{d}_i$ (i=1,2,3) are linearly independent vectors

$$d^{1/2} = \mathbf{d}_1 \times \mathbf{d}_2 \bullet \mathbf{d}_3 > 0 \ . \tag{5.8}$$

In this regard, it should be noted that although the representation (5.1) is exact the expression (5.7) is an approximation of the deformation field in the element.

Now, the element directors can be expressed as functions of the nodal directors using a constant matrix A_{ij} (i,j=0,1,…,7) that is determined by (5.1) and (5.5)

$$\mathbf{D}_i = \sum_{i=0}^{7} A_{ij}\, \bar{\mathbf{D}}_j \ , \quad \mathbf{d}_i = \sum_{i=0}^{7} A_{ij}\, \bar{\mathbf{d}}_j \ . \tag{5.9}$$

In this expression $\bar{\mathbf{d}}_i(t)$ (i=0,1,..,7) are the nodal director vectors that locate the present positions of the nodes of the element. Moreover, the element director velocities $\mathbf{w}_i$ and nodal director velocities $\bar{\mathbf{w}}_i$ are defined by

$$\mathbf{w}_i = \dot{\mathbf{d}}_i \ , \quad \bar{\mathbf{w}}_i = \dot{\bar{\mathbf{d}}}_i \ \ (i=0,1,\ldots,7) \ . \tag{5.10}$$

The objective of the Bubnov-Galerkin approach is to develop weak forms of equations for the director vectors $\mathbf{d}_i$ which represent an approximation of the partial differential equation (4.6b) expressing the balance of linear momentum. To this end, multiply (4.6b) by the weighting function $\phi(\theta^i)$ to deduce that

$$\phi\ m^* \dot{\mathbf{v}}^* = \phi\, m^* \mathbf{b}^* + \sum_{j=1}^{3} [(\phi\, \mathbf{t}^{*j})_{,j} - \mathbf{t}^{*j}\, \phi_{,j}] \ . \tag{5.11}$$

Then, integrate this result over the region P to obtain the weak form

$$\frac{d}{dt}\int_P \phi\, \rho^* \mathbf{v}^*\, dv^* = \int_P \phi\, \rho^* \mathbf{b}^*\, dv^* + \int_{\partial P} \phi\, \mathbf{t}^*\, da^* - \sum_{j=1}^{3} \int_P g^{-1/2}\, \mathbf{t}^{*j}\, \phi_{,j}\, dv^* , \quad (5.12)$$

where use has been made of the conservation of mass (4.6a) and the divergence theorem (4.5).

Next, it is convenient to introduce a number of quantities that are used in the CPE formulation. Specifically, the mass m of the element and the director inertia quantities y^{ij} are given by

$$m = \int_P \rho^* dv^* \ , \ m y^{ij} = \int_P N^i N^j\, \rho^* dv^* = y^{ji} \ (i,j=0,1,\ldots,7) \ , \ y^{00} = 1 \ , \quad (5.13)$$

the external assigned director couples $\mathbf{b}^i$ due to body forces and the director couples $\mathbf{m}^i$ due to surface tractions on the boundaries of the CPE are given by

$$m\mathbf{b}^i = \int_P N^i\, \rho^* \mathbf{b}^*\, dv^* \ , \ \mathbf{m}^i = \int_{\partial P} N^i\, \mathbf{t}^*\, da^* \ (i=0,1,\ldots,7) \ . \quad (5.14)$$

Also, the intrinsic director couples $\mathbf{t}^i$ are expressed by

$$\mathbf{t}^i = \sum_{j=1}^{3} \int_P g^{-1/2}\, \mathbf{t}^{*j}\, N^i{}_{,j}\, dv^* \quad (i=0,1,\ldots,7) \ . \quad (5.15)$$

Then, using these definitions, the global balance laws (4.1)-(4.3), the representation (5.7) and taking ϕ in (5.12) equal to N^i it is possible to derive the balance laws of the CPE. Specifically, the conservation of mass

$$\dot{m} = 0 \ , \quad (5.16)$$

the balances of director momentum

$$\frac{d}{dt}\left(\sum_{j=0}^{7} m y^{ij}\, \mathbf{w}_j\right) = m\mathbf{b}^i + \mathbf{m}^i - \mathbf{t}^i \quad \text{with} \ (\mathbf{t}^0 = 0) \quad (i=0,1,\ldots,7) \ , \quad (5.17)$$

and the balance of angular momentum

$$\frac{d}{dt}\Big(\sum_{i=0}^{7}\sum_{j=0}^{7}\mathbf{d}_i\times m y^{ij}\,\mathbf{w}_j\Big)=\sum_{i=0}^{7}\mathbf{d}_i\times m\mathbf{b}^i+\sum_{i=0}^{7}\mathbf{d}_i\times\mathbf{m}^i\quad(i=0,1,\ldots,7)\ , \tag{5.18}$$

represent the balance laws of the CPE. In particular, it is noted that balances of director momentum (5.17) include the global form (4.2) of the balance of linear momentum for i=0. Also, it can be shown that the director inertia coefficients y^{ij} are constants

$$\dot{y}^{ij}=0\ . \tag{5.19}$$

Furthermore, using the representation (5.7) the rate of work $\mathcal{W}$ and kinetic energy $\mathcal{K}$ in (4.9) can be expressed in the forms

$$\mathcal{W}=\mathcal{W}_b+\mathcal{W}_c\ ,\ \mathcal{W}_b=\sum_{i=0}^{7}m\mathbf{b}^i\bullet\mathbf{w}_i\ ,\ \mathcal{W}_c=\sum_{i=0}^{7}\mathbf{m}^i\bullet\mathbf{w}_i\ ,$$

$$\mathcal{K}=\sum_{i=0}^{7}\sum_{j=0}^{7}\frac{1}{2}m\,y^{ij}\,\mathbf{w}_i\bullet\mathbf{w}_j\ , \tag{5.20}$$

where $\{\mathcal{W}_b,\ \mathcal{W}_c\}$ represent the rates of work done by body forces and surface tractions, respectively.

The main difference between the Bubnov-Galerkin approach and the CPE approach is the procedure for determining constitutive equations for the intrinsic director couples $\mathbf{t}^i$. This will be discussed in detail in the following sections.

6. Balance laws for a 3-D brick CPE (direct approach)

The nodes of the 3-D brick CPE shown in Fig. 5.1 are characterized by the constant reference nodal directors $\bar{\mathbf{D}}_i$ (i=0,1,…,7) and by the present nodal director vectors $\bar{\mathbf{d}}_i(t)$ (i=0,1,…,7) which are functions of time. Then, the reference element directors $\mathbf{D}_i$ and present element directors $\mathbf{d}_i(t)$ are determined by the expressions (5.9) where A_{ij} is a constant matrix. Moreover, the element director velocities $\mathbf{w}_i$ and nodal director velocities $\bar{\mathbf{w}}_i$ are given by (5.10).

In view of the restrictions (5.3) and (5.8) it is possible to define reciprocal vectors $\mathbf{D}^i$ and $\mathbf{d}^i$ (i=1,2,3) by formulas of the type (2.18) and (2.24) so that

$$\mathbf{D}_i \bullet \mathbf{D}^j = \delta_i^{\ j} \ , \ \mathbf{d}_i \bullet \mathbf{d}^j = \delta_i^{\ j} \ , \ (i,j=1,2,3) \ . \tag{6.1}$$

Then, the kinematics of the CPE can be characterized by the deformation tensor $\mathbf{F}$ and its determinant J

$$\mathbf{F} = \mathbf{F}(t) = \sum_{i=1}^{3} \mathbf{d}_i \otimes \mathbf{D}^i \ , \quad J = \det(\mathbf{F}) = \frac{d^{1/2}}{D^{1/2}} > 0 \ , \tag{6.2}$$

associated with homogeneous deformations and the vectors $\boldsymbol{\beta}_i$

$$\boldsymbol{\beta}_i = \mathbf{F}^{-1}\mathbf{d}_{i+3} - \mathbf{D}_{i+3} \ , \ \mathbf{d}_{i+3} = \mathbf{F}(\mathbf{D}_{i+3} + \boldsymbol{\beta}_i) \quad (i=1,2,3,4) \ , \tag{6.3}$$

associated with inhomogeneous deformations. Furthermore, the rate of deformation tensor $\mathbf{L}$ and its symmetric part $\mathbf{D}$ are defined by

$$\mathbf{L} = \dot{\mathbf{F}}\mathbf{F}^{-1} = \sum_{i=1}^{3} \mathbf{w}_i \otimes \mathbf{d}^i \ , \quad \mathbf{D} = \frac{1}{2}(\mathbf{L} + \mathbf{L}^T) = \mathbf{D}^T \ , \tag{6.4}$$

so that

$$\mathbf{w}_i = \mathbf{L}\mathbf{d}_i \ \ (i=1,2,3) \ , \ \mathbf{w}_{i+3} = \mathbf{L}\mathbf{d}_{i+3} + \mathbf{F}\,\dot{\boldsymbol{\beta}}_i \ , \ \dot{\boldsymbol{\beta}}_i = \mathbf{F}^{-1}(\mathbf{w}_{i+3} - \mathbf{L}\mathbf{d}_{i+3}) \ \ (i=1,2,3,4) \ . \quad (6.5)$$

Within the context of the direct approach, the balance laws of the CPE are proposed as the conservation of mass (5.16), the balances of director momentum (5.17) and the balance of angular momentum (5.18). Also, the director inertia coefficients y^{ij} are constants (5.19) and the expressions for the rate of work $\mathtt{W}$ done on the CPE and its kinetic energy $\mathtt{K}$ are given by (2.20). Moreover, the rate of material dissipation $\mathscr{D}$ is proposed by an equation like (4.10), such that

$$d^{1/2}\mathscr{D} = \mathscr{W} - \dot{\mathscr{K}} - m\dot{\Sigma} \geq 0 \ , \quad (6.6)$$

where Σ is the strain energy function per unit mass m of the CPE.

Using the symmetry of the director inertia coefficients y^{ij}, the balances of director momentum (5.17) and introducing the tensor

$$d^{1/2}\mathbf{T} = \sum_{i=1}^{7} \mathbf{t}^i \otimes \mathbf{d}_i \ , \quad (6.7)$$

it can be shown that the reduced form of the balance of angular momentum (5.18) requires $\mathbf{T}$ to be a symmetric tensor

$$\mathbf{T}^T = \mathbf{T} \ , \quad (6.8)$$

which is similar to the restriction (4.8) associated with the three-dimensional theory.

Moreover, using the balances of director momentum (5.17), the rate of material dissipation can be expressed in the form

$$d^{1/2}\mathscr{D} = \sum_{i=1}^{7} \mathbf{t}^i \bullet \mathbf{w}_i - m\dot{\Sigma} \geq 0 \ . \quad (6.9)$$

However, with the help of (6.5) the mechanical power can be rewritten in the form

$$\sum_{i=1}^{7} \mathbf{t}^i \bullet \mathbf{w}_i = d^{1/2}\mathbf{T} \bullet \mathbf{D} + \sum_{i=1}^{4} \mathbf{F}^T\mathbf{t}^{(i+3)} \bullet \dot{\boldsymbol{\beta}}_i \ , \tag{6.10}$$

so the rate of material dissipation reduces to

$$d^{1/2}\mathcal{D} = d^{1/2}\mathbf{T} \bullet \mathbf{D} + \sum_{i=1}^{4} \mathbf{F}^T\mathbf{t}^{(i+3)} \bullet \dot{\boldsymbol{\beta}}_i - m\dot{\Sigma} \geq 0 \ . \tag{6.11}$$

Now, comparison of (6.11) with the three-dimensional equation (4.11) suggests that $d^{1/2}\mathbf{T}$ is similar to the Cauchy stress. In fact, using the approximation (5.7) it follows that

$$\mathbf{g}_j = \sum_{i=1}^{7} N^i{}_{,j}\, \mathbf{d}_i \ . \tag{6.12}$$

Thus, with the help of (2.22), (4.7), (5.15) and (6.7) it can be shown that $d^{1/2}\mathbf{T}$ is related to the volume integral of Cauchy stress $\mathbf{T}^*$

$$d^{1/2}\mathbf{T} = \sum_{i=1}^{7} \sum_{j=1}^{3} \int_P g^{-1/2}\, \mathbf{t}^{*j}\, N^i{}_{,j}\, dv^* \otimes \mathbf{d}_i = \int_P \mathbf{T}^* \left(\sum_{j=1}^{3} \mathbf{g}^j \otimes \mathbf{g}_j\right) dv^* \ ,$$

$$d^{1/2}\mathbf{T} = \int_P \mathbf{T}^*\, dv^* \ . \tag{6.13}$$

Consequently, the volume averaged Cauchy stress $\mathbf{T}^*_{avg}$ is given by

$$\mathbf{T}^*_{avg} = \frac{1}{v^*}\, d^{1/2}\mathbf{T} \ , \tag{6.14}$$

where with the help of (2.17), (3.5) and (5.7) the current volume of the element is given by

$$v^* = \int_P dv^* = H_1H_2H_3 \left[d^{1/2} + \frac{H_1^2}{12}\, \mathbf{d}_4 \times \mathbf{d}_5 \bullet \mathbf{d}_1 + \frac{H_2^2}{12}\, \mathbf{d}_6 \times \mathbf{d}_4 \bullet \mathbf{d}_2 + \frac{H_3^2}{12}\, \mathbf{d}_5 \times \mathbf{d}_6 \bullet \mathbf{d}_3\right] \ . \tag{6.15}$$

7. Constitutive equations for a hyperelastic CPE

The strain energy function Σ^* in (4.12) for a hyperelastic material is local in the sense that it characterizes the response of the material at a material point. In contrast, the 3-D brick CPE is a structure whose response depends on both the material and geometric properties and the structure. Consequently, the constitutive equations for the CPE necessarily combine material and geometric quantities.

A hyperelastic CPE is an ideal element in the same sense that a hyperelastic material is an ideal material. In particular, for a hyperelastic CPE it is assumed that the strain energy function Σ depends tacitly on the reference geometry of the CPE and explicitly on the deformations measures $\{\mathbf{C}, \boldsymbol{\beta}_i\}$

$$\Sigma = \Sigma(\mathbf{C},\boldsymbol{\beta}_i) \ . \tag{7.1}$$

Furthermore, the kinetic quantities $\{\mathbf{T}, \mathbf{t}^i\}$ are assumed to be independent of deformation rates and the rate of dissipation $\mathcal{D}$ in (6.11) is assumed to vanish for all processes

$$d^{1/2}\mathcal{D} = d^{1/2}\mathbf{T} \bullet \mathbf{D} + \sum_{i=1}^{4} \mathbf{F}^T\mathbf{t}^{(i+3)} \bullet \dot{\boldsymbol{\beta}}_i - m\dot{\Sigma} = 0 \ . \tag{7.2}$$

Then, using the usual arguments it can be shown that the kinetic quantities are determined by derivatives of Σ

$$d^{1/2}\mathbf{T} = 2m\mathbf{F}\frac{\partial\Sigma}{\partial\mathbf{C}}\mathbf{F}^T \ , \ \mathbf{t}^{(i+3)} = m\mathbf{F}^{-T}\frac{\partial\Sigma}{\partial\boldsymbol{\beta}_i} \ (i=1,2,3,4) \ , \tag{7.3}$$

with the remaining $\mathbf{t}^i$ (i=0,1,2,3) being determined by (5.17) and (6.7)

$$\mathbf{t}^0 = 0 \ , \ \mathbf{t}^i = [d^{1/2}\mathbf{T} - \sum_{j=4}^{7} \mathbf{t}^j\otimes\mathbf{d}_j] \bullet \mathbf{d}^i \quad (i=1,2,3) \ . \tag{7.4}$$

8. A nonlinear patch test

Following previous research on shells (Naghdi and Rubin, 1995), rods (Rubin, 1996) and points (Rubin, 2000, 2001; Nadler and Rubin, 2003) it is possible to impose restrictions on the strain energy function Σ which ensure that the CPE produces solutions that are consistent with the exact three-dimensional theory for all homogeneous deformations of an arbitrary uniform homogeneous anisotropic elastic materials. These restrictions are equivalent to a nonlinear patch test on the brick element. Specifically, confining attention to such a material it can be shown that the mass m is given by

$$m = \rho_0^* V^* , \tag{8.1}$$

where the volume V^* of the CPE in its reference configuration is determined by using the representation (5.1) to deduce that

$$V^* = D^{1/2} V = \int_{P_0} dV^* ,$$

$$V^* = H_1 H_2 H_3 [D^{1/2} + \frac{H_1^2}{12} \mathbf{D}_4 \times \mathbf{D}_5 \cdot \mathbf{D}_1 + \frac{H_2^2}{12} \mathbf{D}_6 \times \mathbf{D}_4 \cdot \mathbf{D}_2 + \frac{H_3^2}{12} \mathbf{D}_5 \times \mathbf{D}_6 \cdot \mathbf{D}_3] \quad , \tag{8.2}$$

and the quantity V has been introduced for convenience.

Now, using (3.3) and the kinematic assumption (5.7) it can be shown that

$$\mathbf{F}^* = \sum_{m=0}^{3} [\mathbf{F}\mathbf{D}_i + \sum_{i=1}^{4} N^{(i+3)}{}_{,m} \, \mathbf{F}(\mathbf{D}_{i+3} + \boldsymbol{\beta}_i)] \otimes \mathbf{G}^m \quad ,$$

$$\mathbf{F}^* = \mathbf{F} \sum_{m=0}^{3} [\mathbf{G}_m \otimes \mathbf{G}^m + \sum_{i=1}^{4} N^{(i+3)}{}_{,m} \, \boldsymbol{\beta}_i \otimes \mathbf{G}^m] \quad ,$$

$$\mathbf{F}^* = \mathbf{F}[\mathbf{I} + \sum_{i=1}^{4} \sum_{m=0}^{3} N^{(i+3)}{}_{,m} \, \boldsymbol{\beta}_i \otimes \mathbf{G}^m] \quad . \tag{8.3}$$

Thus, the deformation will be three-dimensionally homogeneous with $\mathbf{F}^*$ being independent of the coordinates θ^i if β_i vanish

$$\mathbf{F}^* = \mathbf{F}(t) \text{ for } \beta_i = 0 \ (i=1,2,3,4) \ . \tag{8.4}$$

This result demonstrates that β_i are measures of inhomogeneous deformation. Moreover, Nadler and Rubin (2003) introduced the auxiliary deformation measure $\bar{\mathbf{F}}$

$$\bar{\mathbf{F}} = \mathbf{F}(\mathbf{I} + \sum_{i=1}^{4} \beta_i \otimes \mathbf{V}^i) \ , \tag{8.5}$$

where the vectors $\mathbf{V}^i$ are defined by the reference geometry of the CPE such that

$$D^{1/2} V\mathbf{V}^i = \sum_{m=1}^{3} \int_{P_0} [N^{(i+3)}{}_{,m} \mathbf{G}^m] \, dV^* \ , \quad (i=1,2,3,4) \ . \tag{8.6}$$

Consequently, with the help of (5.1), $\mathbf{V}^i$ are given by

$$D^{1/2} V\mathbf{V}^1 = H_1 H_2 H_3 \, [\frac{H_1^2}{12} \mathbf{D}_5 \times \mathbf{D}_1 + \frac{H_2^2}{12} \mathbf{D}_2 \times \mathbf{D}_6] \ ,$$

$$D^{1/2} V\mathbf{V}^2 = H_1 H_2 H_3 \, [\frac{H_1^2}{12} \mathbf{D}_1 \times \mathbf{D}_4 + \frac{H_3^2}{12} \mathbf{D}_6 \times \mathbf{D}_3] \ ,$$

$$D^{1/2} V\mathbf{V}^3 = H_1 H_2 H_3 \, [\frac{H_2^2}{12} \mathbf{D}_4 \times \mathbf{D}_2 + \frac{H_3^2}{12} \mathbf{D}_3 \times \mathbf{D}_5] \ , \quad D^{1/2} V\mathbf{V}^4 = 0 \ . \tag{8.7}$$

Also, integration of (8.3) over the region P_0 yields the result that $\bar{\mathbf{F}}$ is the volume averaged three-dimensional deformation gradient (Loehnert et al., 2005)

$$\bar{\mathbf{F}} = \int_{P_0} \mathbf{F}^* \, dV^* \ . \tag{8.8}$$

Furthermore, for homogeneous deformations (8.4) of a hyperelastic material the Cauchy stress $\mathbf{T}^*$ is also independent of the coordinates. Consequently, with the help of (3.4), (4.6a), (4.13), (6.15), (8.1) and (8.2) it can be shown that for homogeneous deformations (6.13) requires

$$d^{1/2}\mathbf{T} = v^*\,\mathbf{T}^* = D^{1/2}V\,J^*\,\mathbf{T}^* = 2m\,\mathbf{F}^*\frac{\partial\Sigma^*}{\partial\mathbf{C}^*}\mathbf{F}^{*T} = 2m\,\mathbf{F}\frac{\partial\Sigma^*(\mathbf{C})}{\partial\mathbf{C}}\mathbf{F}^T\,. \tag{8.9}$$

Also, for homogeneous deformations (5.15) yields

$$\mathbf{t}^{(i+3)} = \sum_{m=1}^{3}\int_P \mathbf{T}^*\mathbf{g}^m\,N^{(i+3)}{}_{,m}\,dv^* = J\,\mathbf{T}^*\mathbf{F}^{-T}\int_{P_0}\sum_{m=1}^{3} N^{(i+3)}{}_{,m}\,\mathbf{G}^m\,dV^*\,,$$

$$\mathbf{t}^{(i+3)} = D^{1/2}V\,J\,\mathbf{T}^*\mathbf{F}^{-T}\,\mathbf{V}^i = d^{1/2}\mathbf{T}\,\mathbf{F}^{-T}\mathbf{V}^i \quad (i=1,2,3,4)\,. \tag{8.10}$$

Now, comparison of the results (8.9) and (8.10) with the constitutive equations (7.3) indicates that the CPE will satisfy the patch test provided that the strain energy function satisfies the restrictions that

$$\frac{\partial\Sigma}{\partial\mathbf{C}} = \frac{\partial\Sigma^*(\mathbf{C})}{\partial\mathbf{C}}\,,\quad \frac{\partial\Sigma}{\partial\boldsymbol{\beta}_i} = 2\,\mathbf{C}\frac{\partial\Sigma^*(\mathbf{C})}{\partial\mathbf{C}}\mathbf{V}^i \quad (i=1,2,3,4) \quad \text{for } \boldsymbol{\beta}_i = 0\,. \tag{8.11}$$

Motivated by the work in (Nadler and Rubin, 2003) these restrictions can be simplified by writing the general form of the strain energy of the CPE as

$$\Sigma(\mathbf{C},\boldsymbol{\beta}_i) = \Sigma^*(\bar{\mathbf{C}}) + \Psi(\bar{\mathbf{C}},\boldsymbol{\beta}_i) \qquad (i=1,2,3,4)\,, \tag{8.12}$$

where here Ψ is taken to be a function of $\{\bar{\mathbf{C}},\boldsymbol{\beta}_i\}$ instead of $\{\mathbf{C},\boldsymbol{\beta}_i\}$ as in (Nadler and Rubin, 2003). Next, taking the material derivative of (8.5) yields the results that

$$\dot{\bar{\mathbf{F}}} = \mathbf{L}\bar{\mathbf{F}} + \mathbf{F}\,(\sum_{i=1}^{4}\dot{\boldsymbol{\beta}}_i\otimes\mathbf{V}^i)\,,$$

$$\dot{\bar{\mathbf{C}}} = \bar{\mathbf{F}}^{T}\mathbf{F}^{-T}\dot{\mathbf{C}}\mathbf{F}^{-1}\bar{\mathbf{F}} + \bar{\mathbf{F}}^{T}\mathbf{F}\,(\sum_{i=1}^{4}\dot{\boldsymbol{\beta}}_i\otimes\mathbf{V}^i) + (\sum_{i=1}^{4}\mathbf{V}^i\otimes\dot{\boldsymbol{\beta}}_i)\,\mathbf{F}^{T}\,\bar{\mathbf{F}}\ , \tag{8.13}$$

so that using the chain rule of differentiation it can be shown that

$$\frac{\partial\Sigma}{\partial\mathbf{C}} = \mathbf{F}^{-1}\bar{\mathbf{F}}\,[\frac{\partial\Sigma^{*}(\bar{\mathbf{C}})}{\partial\bar{\mathbf{C}}} + \frac{\partial\Psi}{\partial\bar{\mathbf{C}}}]\,\bar{\mathbf{F}}^{T}\mathbf{F}^{-T}\ ,$$

$$\frac{\partial\Sigma}{\partial\boldsymbol{\beta}_i} = \frac{\partial\Psi}{\partial\boldsymbol{\beta}_i} + 2\,\mathbf{F}^{T}\bar{\mathbf{F}}\ [\frac{\partial\Sigma^{*}(\bar{\mathbf{C}})}{\partial\bar{\mathbf{C}}} + \frac{\partial\Psi}{\partial\bar{\mathbf{C}}}]\,\mathbf{V}^i\ \ (i=1,2,3,4)\ . \tag{8.14}$$

Thus, with the help of the representation (8.12) the restrictions (8.11) reduce to restrictions on only the inhomogeneous part Ψ of the strain energy

$$\frac{\partial\Psi(\bar{\mathbf{C}},\boldsymbol{\beta}_i)}{\partial\bar{\mathbf{C}}} = 0\ ,\ \frac{\partial\Psi(\bar{\mathbf{C}},\boldsymbol{\beta}_i)}{\partial\boldsymbol{\beta}_m} = 0\quad \text{for } \boldsymbol{\beta}_i = 0\quad (i,m=1,2,3,4)\ . \tag{8.15}$$

For general anisotropic materials it is not known how to propose a functional form for Ψ which includes dependence on the reference geometry that causes the CPE to produce accurate results for general irregular shaped elements experiencing bending dominated loads. However, progress made for isotropic materials will be discussed in the next sections.

9. A specific form of the strain energy function for inhomogeneous deformations

Using the definitions of the inhomogeneous strain measures κ_j^i in (Nadler and Rubin, 2003; Jabareen and Rubin, 2007e)

$$\kappa_1^1 = H_2\,\boldsymbol{\beta}_1 \bullet \mathbf{D}^1 \;,\; \kappa_1^2 = H_1\,\boldsymbol{\beta}_1 \bullet \mathbf{D}^2 \;,\; \kappa_1^3 = H_3\,\boldsymbol{\beta}_1 \bullet \mathbf{D}^3 \;,$$

$$\kappa_2^1 = H_3\,\boldsymbol{\beta}_2 \bullet \mathbf{D}^1 \;,\; \kappa_2^2 = H_2\,\boldsymbol{\beta}_2 \bullet \mathbf{D}^2 \;,\; \kappa_2^3 = H_1\,\boldsymbol{\beta}_2 \bullet \mathbf{D}^3 \;,$$

$$\kappa_3^1 = H_1\,\boldsymbol{\beta}_3 \bullet \mathbf{D}^1 \;,\; \kappa_3^2 = H_3\,\boldsymbol{\beta}_3 \bullet \mathbf{D}^2 \;,\; \kappa_3^3 = H_2\,\boldsymbol{\beta}_3 \bullet \mathbf{D}^3 \;,$$

$$\kappa_4^1 = H_2H_3\,\boldsymbol{\beta}_4 \bullet \mathbf{D}^1 \;,\; \kappa_4^2 = H_1H_3\,\boldsymbol{\beta}_4 \bullet \mathbf{D}^2 \;,\; \kappa_4^3 = H_1H_2\,\boldsymbol{\beta}_4 \bullet \mathbf{D}^3 \;, \tag{9.1}$$

and the alternative variables b_i (i=1,2,…,12) defined by

$$b_i = \{\kappa_1^1, \kappa_3^3, \kappa_1^2, \kappa_2^3, \kappa_2^1, \kappa_3^2, \kappa_1^3, \kappa_2^2, \kappa_3^1, \kappa_4^1, \kappa_4^2, \kappa_4^1\} \;, \tag{9.2}$$

it is convenient to replace the dependence of Ψ on $\boldsymbol{\beta}_j$ (j=1,2,3,4) with dependence on b_j and express the strain energy function in the form

$$\Sigma(\mathbf{C},\boldsymbol{\beta}_j) = \Sigma^*(\bar{\mathbf{C}}) + \Psi(\bar{\mathbf{C}},b_i) \qquad (i=1,2,\ldots,12) \;. \tag{9.3}$$

Then, the constitutive equations for a hyperelastic CPE become

$$d^{1/2}\mathbf{T} = 2m\,\bar{\mathbf{F}}\,[\frac{\partial\Sigma^*(\bar{\mathbf{C}})}{\partial\bar{\mathbf{C}}} + \frac{\partial\Psi}{\partial\bar{\mathbf{C}}}]\,\bar{\mathbf{F}}^T \;,$$

$$\mathbf{t}^4 = [m\,\frac{\partial\Psi}{\partial b_1}\,H_2\mathbf{d}^1 + m\,\frac{\partial\Psi}{\partial b_3}\,H_1\mathbf{d}^2 + m\,\frac{\partial\Psi}{\partial b_7}\,H_3\mathbf{d}^3] + (d^{1/2}\mathbf{T})(\bar{\mathbf{F}}^{-T}\,\mathbf{V}^1) \;,$$

$$\mathbf{t}^5 = [m\,\frac{\partial\Psi}{\partial b_5}\,H_3\mathbf{d}^1 + m\,\frac{\partial\Psi}{\partial b_8}\,H_2\mathbf{d}^2 + m\,\frac{\partial\Psi}{\partial b_4}\,H_1\mathbf{d}^3] + (d^{1/2}\mathbf{T})(\bar{\mathbf{F}}^{-T}\,\mathbf{V}^2) \;,$$

$$\mathbf{t}^6 = [m\,\frac{\partial\Psi}{\partial b_9}\,H_1\mathbf{d}^1 + m\,\frac{\partial\Psi}{\partial b_6}\,H_3\mathbf{d}^2 + m\,\frac{\partial\Psi}{\partial b_2}\,H_2\mathbf{d}^3] + (d^{1/2}\mathbf{T})(\bar{\mathbf{F}}^{-T}\,\mathbf{V}^3) \;,$$

$$\mathbf{t}^7 = [m\,\frac{\partial\Psi(\bar{\mathbf{C}},\kappa_j^i)}{\partial\kappa_4^1}\,H_2H_3\mathbf{d}^1 + m\,\frac{\partial\Psi(\bar{\mathbf{C}},\kappa_j^i)}{\partial\kappa_4^2}\,H_1H_3\mathbf{d}^2 + m\,\frac{\partial\Psi(\bar{\mathbf{C}},\kappa_j^i)}{\partial\kappa_4^3}\,H_1H_2\mathbf{d}^3]\,, \quad (9.4)$$

with the remaining expressions for $\mathbf{t}^i$ (i=0,1,2,3) are given by (7.4). Moreover, the special case considered in (Jabareen and Rubin, 2007e) takes Ψ to be a quadratic function of b_i which is independent of $\bar{\mathbf{C}}$, such that

$$2m\Psi = \frac{D^{1/2}V\mu}{6(1-\nu)}\,[\sum_{i=1}^{12}\sum_{j=1}^{12} B_{ij}\,b_i\,b_j]\,, \quad (9.5)$$

where $\{\mu,\ \nu\}$ are the shear modulus and Poisson's ratio associated with the small deformation response and B_{ij} is a symmetric matrix. As a special case, higher-order hourglass modes are uncoupled from bending and torsional modes so that (Nadler and Rubin, 2003)

$$B_{ij} = 0 \ \text{ for i=10 and j}\neq 10\ ,\ B_{ij} = 0 \text{ for i=11 and j}\neq 11\ ,$$

$$B_{ij} = 0 \text{ for i=12 and j}\neq 12\ ,$$

$$B_{(10,10)} = \frac{(1-\nu)}{24}\,[\frac{2(3-\nu)}{(3-2\nu)} + \frac{H_1^2}{H_2^2} + \frac{H_1^2}{H_3^2}]\,,\ B_{(11,11)} = \frac{(1-\nu)}{24}\,[\frac{2(3-\nu)}{(3-2\nu)} + \frac{H_2^2}{H_1^2} + \frac{H_2^2}{H_3^2}]\,,$$

$$B_{(12,12)} = \frac{(1-\nu)}{24}\,[\frac{2(3-\nu)}{(3-2\nu)} + \frac{H_3^2}{H_1^2} + \frac{H_3^2}{H_2^2}]\,. \quad (9.6)$$

The remaining 45 values of B_{ij} need to be determine by matching exact solutions to specific problems.

10. Determination of the constitutive coefficients

The coefficients B_{ij} of the strain energy Ψ of inhomogeneous deformations (9.5) can be determined by matching exact solutions of the linearized theory of an isotropic elastic material. Specifically, these coefficients were determined in (Nadler and Rubin, 2003) by matching exact solutions of pure bending and pure torsion of a rectangular parallelepiped. Then, the same functional forms of B_{ij} were used for elements with general reference shapes. In (Loehnert et al., 2005) it was shown that the resulting CPE exhibited robust, accurate response to a number of problems which typically exhibit unphysical locking or hourglassing in other element formulations. However, it was also shown there that the CPE exhibited undesirable sensitivity to irregularity of the reference element shape.

Recently, Boerner et al. (2007) have proposed a numerical method for determining coefficients in a quadratic form of the strain energy function for inhomogeneous deformations of a 2-D plane strain formulation of the CPE. This numerical approach produces improved response for irregular shaped elements. Jabareen and Rubin (2007b) developed analytical forms for B_{ij} which cause an improved 3-D brick CPE to yield results that are relatively insensitive to element irregularity for a number of problems. However, it was observed that the accuracy of this improved CPE for out-of-plane bending of a rhombic plate degrades as the angle of plate decreases from 90°. This is because the coefficients developed in (Jabareen and Rubin, 2007b) were not based on out-of-plane bending solutions. Later, Jabareen and Rubin (2007e) developed a generalized CPE which removed the deficiency in the improved CPE. Specifically, the functional forms for B_{ij} were generalized to include full coupling of bending and

torsional modes of deformation. Also, the generalized CPE was obtained by considering out-of-plane bending solutions in addition to in-plane bending solutions.

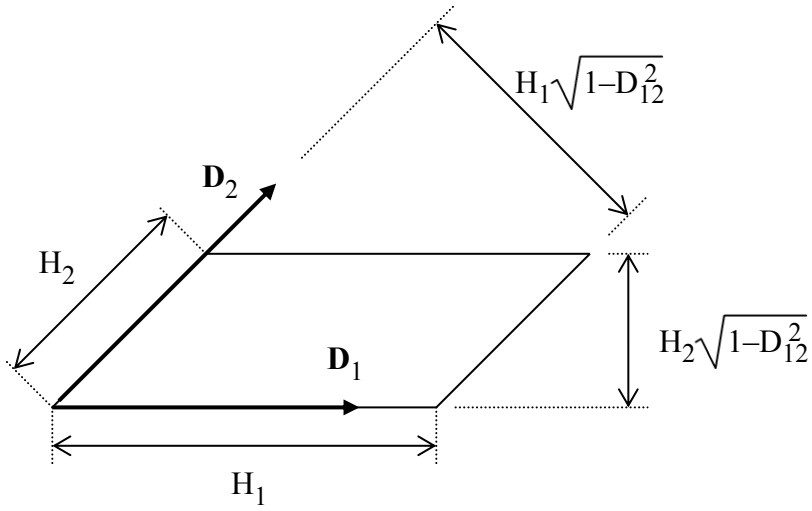

Fig. 10.1 Sketch of the cross-section of the parallelepiped element E1.

It was observed in (Jabareen and Rubin, 2007b,e) that in order to develop functional forms for B_{ij} which produce a CPE that is relatively insensitive to element irregularity it is sufficient to focus attention on the bending and torsion response of elements which are parallelepipeds with two right angles. Specifically, with reference to the base vectors $\mathbf{e}_i$ of a fixed rectangular Cartesian coordinate system it is convenient to introduce the metric D_{ij}

$$D_{ij} = \mathbf{D}_i \bullet \mathbf{D}_j \ , \tag{10.1}$$

and consider the three elements E1-E3 defined by (see Fig. 10.1 for E1)

Element E1 ($D_{12}\neq 0$, $D_{13}=0$, $D_{23}=0$)

$$\mathbf{D}_1 = \mathbf{e}_1 \ , \ \mathbf{D}_2 = D_{12}\, \mathbf{e}_1 + \sqrt{1-D_{12}^2}\, \mathbf{e}_2 \ , \ \mathbf{D}_3 = \mathbf{e}_3 \ , \mathbf{D}_i = 0 \ (i=0,4,5,6,7) \ , \tag{10.2a}$$

Element E2 ($D_{12}=0$, $D_{13}\neq 0$, $D_{23}=0$)

$$\mathbf{D}_1 = \mathbf{e}_1 \ , \ \mathbf{D}_2 = \mathbf{e}_2 \ , \ \mathbf{D}_3 = D_{13}\,\mathbf{e}_1 + \sqrt{1-D_{13}^2}\,\mathbf{e}_3 \ , \ \mathbf{D}_i = 0 \ (i=0,4,5,6,7) \ , \quad (10.2b)$$

Element E3 ($D_{12}=0$, $D_{13}=0$, $D_{23}\neq 0$)

$$\mathbf{D}_1 = \mathbf{e}_1 \ , \ \mathbf{D}_2 = \mathbf{e}_2 \ , \ \mathbf{D}_3 = D_{23}\,\mathbf{e}_2 + \sqrt{1-D_{23}^2}\,\mathbf{e}_3 \ , \ \mathbf{D}_i = 0 \ (i=0,4,5,6,7) \ . \quad (10.2c)$$

It then follows from (8.2) and (8.7) that for these elements

$$V = H_1 H_2 H_3 \ , \ \mathbf{V}^i = 0 \ \ (i=1,2,3,4) \ , \quad (10.3)$$

and the position vector $\mathbf{X}^*$ in (5.1) reduces to

$$\mathbf{X}^* = \sum_{j=1}^{3} \theta^j \, \mathbf{D}_j \ , \quad (10.4)$$

where $\mathbf{D}_0$ has been set equal to zero. Also, for the example problems considered in this section use is made of linearized constitutive equations associated with the compressible Neo-Hookean strain energy function (4.18).

Now, with reference to the base vectors $\mathbf{e}_i'$ of another fixed rectangular Cartesian coordinate system, the components $\{X_i^{*\prime},\ u_i^{*\prime},\ T_{ij}^{*\prime}\}$ of the position vector $\mathbf{X}^*$, the displacement vector $\mathbf{u}^*$ and the stress tensor $\mathbf{T}^*$, respectively, of an exact solution of the linear equations of elasticity can be expressed in the forms

$$\mathbf{X}^* = \sum_{i=1}^{3} X_i^{*\prime}\,\mathbf{e}_i' \ , \quad \mathbf{u}^* = \sum_{i=1}^{3} u_i^{*\prime}\,\mathbf{e}_i' \ , \quad \mathbf{T}^* = \sum_{i=1}^{3}\sum_{j=1}^{3} T_{ij}^{*\prime}\,(\mathbf{e}_i'\otimes\mathbf{e}_j') \ . \quad (10.5)$$

Moreover, the classical pure bending solution (e.g. Sokolnikoff, 1956) of the three dimensional equations of isotropic elasticity for a rectangular parallelepiped can be written in the form

$$\mathbf{u}^* = (\gamma\, X_1^{*\prime}\, X_2^{*\prime})\, \mathbf{e}_1' - \frac{1}{2}\gamma\, [(X_1^{*\prime})^2 + \nu\, (X_2^{*\prime})^2 - \nu\, (X_3^{*\prime})^2]\, \mathbf{e}_2' - (\gamma\, \nu\, X_2^{*\prime}\, X_3^{*\prime})\, \mathbf{e}_3' \,,$$

$$\mathbf{T}^* = 2\mu(1+\nu^*)\gamma\ X_2^{*\prime}\ (\mathbf{e}_1' \otimes \mathbf{e}_1') \ , \tag{10.6}$$

where γ controls the magnitude of the pure bending. Similarly, the simple torsion-like solution in (Jabareen and Rubin, 2007c) can be expressed in the form

$$\mathbf{u}^* = (-\omega\ \phi\, X_2^{*\prime} X_3^{*\prime})\, \mathbf{e}_1' + (-\omega\ X_1^{*\prime} X_3^{*\prime})\ \mathbf{e}_2' + (\omega\ X_1^{*\prime} X_2^{*\prime})\, \mathbf{e}_3' \ ,$$

$$\mathbf{T}^* = \mu\omega\, [-(1+\phi) X_3^{*\prime}\, (\mathbf{e}_1' \otimes \mathbf{e}_2' + \mathbf{e}_2' \otimes \mathbf{e}_1') + (1-\phi) X_2^{*\prime}\, (\mathbf{e}_1' \otimes \mathbf{e}_3' + \mathbf{e}_3' \otimes \mathbf{e}_1')] \,, \tag{10.7}$$

where the constant ω is the twist per unit length in the $\mathbf{e}_1'$ direction and the constant ϕ controls the warping of the cross-section with unit normal $\mathbf{e}_1'$. Moreover, with the help of (10.4) and (10.5) the components $X_i^{*\prime}$ are determined by the convected coordinates θ^j

$$X_i^{*\prime} = \sum_{j=1}^{3}\ (\mathbf{e}_i' \bullet \mathbf{D}_j)\ \theta^j \,, \tag{10.8}$$

so that the solutions (10.6) and (10.7) can be expressed as function of θ^j.

Within the context of the linear theory of a CPE (Nadler and Rubin, 2003) the director displacements $\boldsymbol{\delta}_i$ are defined such that

$$\mathbf{d}_i = \mathbf{D}_i + \boldsymbol{\delta}_i \ , (i=0,1,\ldots,7) \ , \tag{10.9}$$

and for the special elements defined by (10.2) the linearized forms of the inhomogeneous strains $\boldsymbol{\beta}_i$ become

$$\boldsymbol{\beta}_i = \boldsymbol{\delta}_{i+3} \quad (i=1,2,3,4) \ . \tag{10.10}$$

As explained in (Nadler and Rubin, 2003), the values $\boldsymbol{\delta}_i^*$ of the element director displacements $\boldsymbol{\delta}_i$ which correspond to the exact displacement field $\mathbf{u}^*$ need to be properly

defined. Specifically, for these element shapes the values δ_i^* are determined by the equations in (Nadler and Rubin, 2003) which connect δ_i^* to integrals over the reference element region P_0 of derivatives of $\mathbf{u}^*$ with respect to the convected coordinates

$$\delta_0^* = \frac{1}{V^*}\int_P \mathbf{u}^*\, dV^* \ , \ \delta_i^* = \frac{1}{V^*}\int_P \frac{\partial \mathbf{u}^*}{\partial \theta^i}\, dV^* \ \ (i=1,2,3) \ ,$$

$$\delta_4^* = \frac{1}{V^*}\int_P \frac{\partial^2 \mathbf{u}^*}{\partial \theta^1 \partial \theta^2}\, dV^* \ , \ \delta_5^* = \frac{1}{V^*}\int_P \frac{\partial^2 \mathbf{u}^*}{\partial \theta^1 \partial \theta^3}\, dV^* \ ,$$

$$\delta_6^* = \frac{1}{V^*}\int_P \frac{\partial^2 \mathbf{u}^*}{\partial \theta^2 \partial \theta^3}\, dV^* \ , \delta_7^* = \frac{1}{V^*}\int_P \frac{\partial^3 \mathbf{u}^*}{\partial \theta^1 \partial \theta^2 \partial \theta^3}\, dV^* \ . \qquad (10.11)$$

In particular, for the exact solutions (10.6) and (10.7) and the element shapes (10.2) it can be shown that these expressions yield

$$\delta_1^* = \delta_2^* = \delta_3^* = \delta_7^* = 0 \ , \qquad (10.12)$$

so that when δ_i are replaced by the exact values δ_i^* the linearized values of κ_4^i vanish

$$\kappa_4^1 = \kappa_4^2 = \kappa_4^3 = 0 \ , \qquad (10.13)$$

and the with the help of (7.4) and (9.5) the linearized forms of the constitutive equations (9.4) reduce to

$$d^{1/2}\mathbf{T} = 0 \ , \ \mathbf{t}^i = 0 \ \ (i=0,1,2,7) \ ,$$

$$\mathbf{t}^4 = \frac{D^{1/2}V\mu}{6(1-\nu)} \sum_{j=1}^{12} [B_{1j}\, H_2 \mathbf{D}^1 + B_{3j}\, H_1 \mathbf{D}^2 + B_{7j}\, H_3 \mathbf{D}^3]\, b_j \ ,$$

$$\mathbf{t}^5 = \frac{D^{1/2}V\mu}{6(1-\nu)} \sum_{j=1}^{12} [B_{5j}\, H_3 \mathbf{D}^1 + B_{8j}\, H_2 \mathbf{D}^2 + B_{4j}\, H_1 \mathbf{D}^3]\, b_j \ ,$$

$$\mathbf{t}^6 = \frac{D^{1/2}V\mu}{6(1-\nu)} \sum_{j=1}^{12} [B_{9j}\, H_1 \mathbf{D}^1 + B_{6j}\, H_3 \mathbf{D}^2 + B_{2j}\, H_2 \mathbf{D}^3]\, b_j \,, \tag{10.14}$$

where $\mathbf{d}^i$ have been replaced by the reference values $\mathbf{D}^i$. Also, the values of $\mathbf{m}^i$ in (5.14) associated with the exact solutions (10.6) and (10.7) are given by

$$\mathbf{m}^i = 0 \;\; (i=0,1,2,3,7) \;\; , \quad \mathbf{m}^i = \int_{\partial P_0} N^i\, \mathbf{T}^*\, \mathbf{N}^*\, dA^* \;\; (i=4,5,6) \,, \tag{10.15}$$

where ∂P_0 is the reference boundary of the CPE, $\mathbf{N}^*$ is the unit outward normal to ∂P_0 and dA^* is the reference element of area. It then follows that within the context of the linearized theory, the equations of equilibrium associated with the bending (10.6) and torsion (10.7) solutions reduce to three vector equations

$$\mathbf{t}^i - \mathbf{m}^i = 0 \;\; (i=4,5,6) \;\; . \tag{10.16}$$

Analytical expressions for B_{ij} can be developed by matching the solutions (10.6) and (10.7) for each of the element shapes (10.2). Specifically, with reference to the element shape E1 in (10.2a) consider six bending solutions associated with specifications of the orientations of $\mathbf{e}_i'$ relative to $\mathbf{D}_i$

Bending B1: $\mathbf{e}_1' = \mathbf{D}_1 \,, \;\; \mathbf{e}_3' = \mathbf{D}_3 \,,$ (10.17a)

Bending B2: $\mathbf{e}_1' = \mathbf{D}_1 \,, \;\; \mathbf{e}_2' = \mathbf{D}_3 \,,$ (10.17b)

Bending B3: $\mathbf{e}_1' = \mathbf{D}_2 \,, \; \mathbf{e}_3' = \mathbf{D}_3 \,,$ (10.17c)

Bending B4: $\mathbf{e}_1' = \mathbf{D}_2 \,, \;\; \mathbf{e}_2' = \mathbf{D}_3 \,,$ (10.17d)

Bending B5: $\mathbf{e}_1' = \mathbf{D}_3 \,, \; \mathbf{e}_3' = \mathbf{D}_2 \,,$ (10.17e)

Bending B6: $\mathbf{e}_1' = \mathbf{D}_3 \,, \; \mathbf{e}_3' = -\mathbf{D}_1 \,.$ (10.17f)

Also, consider two torsion solutions associated with specifications

Torsion T1: $$\mathbf{e}_1' = \mathbf{D}_1 \, , \;\; \mathbf{e}_3' = \mathbf{D}_3 \, , \tag{10.18a}$$

Torsion T2: $$\mathbf{e}_1' = \mathbf{D}_2 \, , \; \mathbf{e}_3' = \mathbf{D}_3 \, . \tag{10.18b}$$

For each bending and torsion solution the exact values δ_i^* are determined by (10.11), the linearized values of κ_j^i are determined using (9.1) and (10.10) with δ_i replaced by δ_i^* and the resulting constitutive equations for $\mathbf{t}^i$ are determined by (10.14). Also, the values of the warping constant ϕ corresponding to nearly pure torsion being determined by

Torsion T1: $$\mathbf{m}^6 \bullet \mathbf{D}_1 = 0 \;\; \Rightarrow \;\; \phi = \frac{H_2^2(1-D_{12}^2)-H_3^2}{H_2^2(1-D_{12}^2)+H_3^2} , \tag{10.19a}$$

Torsion T2: $$\mathbf{m}^5 \bullet \mathbf{D}_2 = 0 \;\; \Rightarrow \;\; \phi = \frac{H_1^2(1-D_{12}^2)-H_3^2}{H_1^2(1-D_{12}^2)+H_3^2} \, . \tag{10.19b}$$

For each bending solution the value of γ can be eliminated in the resulting equations of equilibrium (10.16) and the value of ω can be eliminated from each of the equations of equilibrium associated with the torsion solutions. Also, the values (10.19) are used in the resulting torsion equations. It therefore follows that the each of the solutions (B1)-(B6), (T1) and (T2) yield nine scalar equations of equilibrium which total 72 scalar equations to determine the values of B_{ij} as functions of H_i and D_{12}. Some of these scalar equations are trivially satisfied and others are redundant. In particular, using a symbolic program like Maple it can be shown that these equations can be solved for B_{ij} such that

$$\det(B_{ij}) > 0 \; . \tag{10.20}$$

Similar procedures can be used to define bending and torsion solutions for the element shapes E2 and E3 and the resulting equations can be solved for B_{ij} to determine

the dependence on the metrics D_{13} and D_{23}. Next, introducing the auxiliary variables $\{\lambda_{12}, \lambda_{13}, \lambda_{23}\}$ defined by

For $D_{12}^2+D_{13}^2+D_{23}^2 = 0$:

$$\lambda_{12} = \lambda_{13} = \lambda_{23} = 0 \ , \tag{10.21a}$$

For $D_{12}^2+D_{13}^2+D_{23}^2 > 0$:

$$\lambda_{12} = \frac{D_{12}^2}{D_{12}^2+D_{13}^2+D_{23}^2} \ , \ \lambda_{13} = \frac{D_{13}^2}{D_{13}^2+D_{13}^2+D_{23}^2} \ , \ \lambda_{23} = \frac{D_{23}^2}{D_{13}^2+D_{13}^2+D_{23}^2} \ , \tag{10.21b}$$

it is possible to denote the values of B_{ij} associated with the solutions of the three elements E1-E3 in (10.2) by B_{ij}^{12} for E1, by B_{ij}^{13} for E2, and by B_{ij}^{23} for E3. Also, the matrix B_{ij}^{0} is defined so that it yields a strain energy function Ψ equivalent to that obtained in (Nadler and Rubin, 2003) for a rectangular parallelepiped, when the value of the torsion function $b^*(1)$ is taken to be 1/2 as suggested in (Jabareen and Rubin, 2007c). Then, the general expression $B_{ij}(D_{12},D_{13},D_{23})$ which combines these solutions is given by

$$B_{ij}(D_{12},D_{13},D_{23}) = (1-\lambda_{12}-\lambda_{13}-\lambda_{23})\, B_{ij}^{0} + \lambda_{12}\, B_{ij}^{12} + \lambda_{13}\, B_{ij}^{13} + \lambda_{23}\, B_{ij}^{23} \ . \tag{10.22}$$

Now, using the definitions (10.21) it follows that each of the coefficients $\{(1-\lambda_{12}-\lambda_{13}-\lambda_{23}), \lambda_{12}, \lambda_{13}, \lambda_{23}\}$ is non-negative and that at least one of them is positive. Also, each of the matrices $\{B_{ij}^{0}, B_{ij}^{12}, B_{ij}^{13}, B_{ij}^{23}\}$ is positive definite so that the combined matrix $B_{ij}(D_{12},D_{13},D_{23})$ is also positive definite for all reference element shapes.

11. A test for path-dependence

The formulation of the CPE for nonlinear elasticity treats the element as a structure and determines the kinetic quantities by derivatives of a strain energy function so that the dissipation vanishes. It therefore follows that the CPE formulation is automatically hyperelastic and predicts path-independent results. In contrast, element formulations which modify full integration methods like those associated with enhanced strain or incompatible mode methods can introduce path-dependence of the results. Although an analytical proof is required to ensure that an element formulation is hyperelastic for all deformations, only a single calculation is needed to prove that an element formulation is path-dependent.

Jabareen and Rubin (2007a) introduced a simple simulation which can be used to test element formulations for path-dependence and the elements in Table 1.1 were tested. In the examples considered here and in the rest of the text the elements ABBAQUS-6, ADINA-2, ANSYS-3 and FEAP-3 in Table 1.1 are denoted by (AB), (AD), (F), respectively. Also, the generalized CPE is denoted by (C).

It has been shown in (Jabareen and Rubin, 2007a) that the response of (F) is similar to that of other enhanced strain and incompatible mode elements. Therefore, for most of the example problems presented in the following sections, comparisons will be limited to the element in FEAP. However, the results of the (Q1P0) 3-D brick element and the mixed higher order nine node quadrilateral element [denoted by (HO9)] in FEAP will be used for comparison of some of the examples using nearly incompressible material response.

In order to test potential path-dependency of element formulations, consider a single brick element which is a cube in its reference configuration with edges of length $L = 1$ m

(see Fig. 11.1). The four nodes located by $\mathbf{X}_i$ (i=1,2,3,4) are fixed, the nodes $\mathbf{X}_i$ (i=5,6,7) are free and the node $\mathbf{X}_8$ is deformed to the location $\mathbf{x}_8$ by the displacement $\mathbf{u}_8$

$$\mathbf{x}_8 = \mathbf{X}_8 + \mathbf{u}_8 \ . \tag{11.1}$$

Specifically, the displacement $\mathbf{u}_8$ is characterized by a sequence of straight line segments that connect the end points A-F shown in Fig. 11.1 which are characterized by

$$\mathbf{u}_A = 0 \ , \ \mathbf{u}_B = -\beta \ \mathbf{e}_1 \ , \ \mathbf{u}_C = -\beta \ \mathbf{e}_1 - \beta \ \mathbf{e}_2 \ , \ \mathbf{u}_D = -\beta \ \mathbf{e}_1 - \beta \ \mathbf{e}_2 - \beta \ \mathbf{e}_3 \ ,$$

$$\mathbf{u}_E = -\beta \ \mathbf{e}_2 - \beta \ \mathbf{e}_3 \ , \ \ \mathbf{u}_F = -\beta \ \mathbf{e}_3 \ , \ \beta = 0.25 \text{ m} \ , \tag{11.2}$$

The total external work done on the element is given by

$$W = \int \mathbf{f}_8 \bullet \dot{\mathbf{u}}_8 \, dt \ , \tag{11.3}$$

where $\mathbf{f}_8$ is the external nodal force applied to node 8.

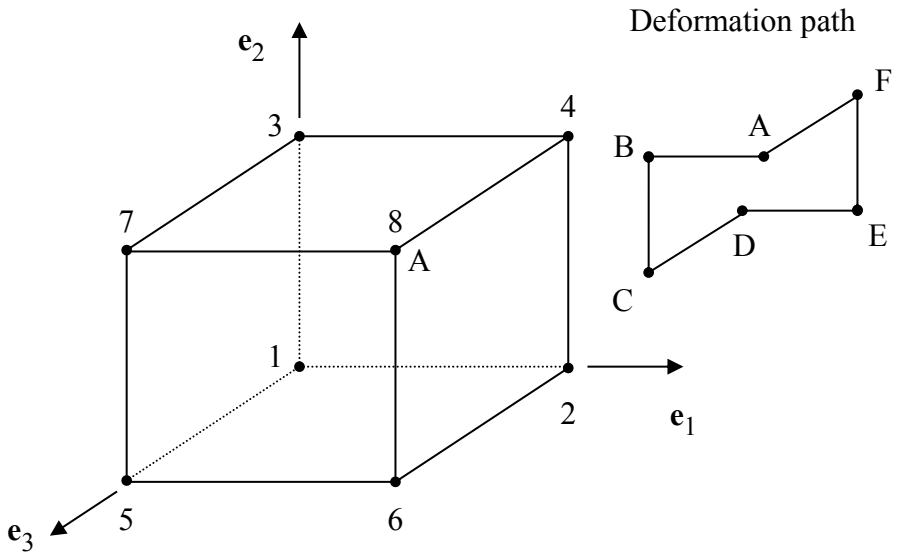

Fig. 11.1 Sketch of the cubical element showing the numbering of the nodes and the paths used to test path-dependency of various element formulations.

To quantify the error associated with path-dependency it is convenient to introduce the quantities

$$W_A^* = W_{ABCDEFA} \ , \quad W_A^{**} = W_{AFEDEFA} \ ,$$

$$W_D^* = W_{ABCD} \ , \ W_D^{**} = W_{AFED} \ ,$$

$$E_A^* = \frac{W_A^*}{W_D^*} \ , \quad E_A^{**} = \frac{W_A^{**}}{W_D^*} \ , \ E_D = \frac{W_D^* - W_D^{**}}{W_D^*} \ . \tag{11.4}$$

Here, W_A^* denotes the work done on the element in a single cycle of deformation following the path ABCDEFA, W_A^{**} denotes the work done in a single cycle of the path AFED and its reverse path DEFA, W_D^* is the work done during the path ABCD and W_D^{**} is the work done during the path AFED to the same point D. Also, E_A^* and E_A^{**} are the relative errors for the cycles associated with W_A^* and W_A^{**}, respectively and E_D is the relative error associated with the two different paths to the point D. The trapezoidal rule was used to integrate (11.3) and each segment of the deformation was divided into N=250 equal steps to ensure accuracy.

Three types of element response are possible: hyperelastic, Cauchy elastic and hypoelastic. For hyperelastic element response the nodal forces maintaining equilibrium of any configuration and the work done between two configurations are both path-independent. For Cauchy elastic element response the nodal forces maintaining equilibrium of any configuration are path-independent but the work done between two configurations is path-dependent. For hypoelastic element response the nodal forces maintaining equilibrium of any configuration and the work done between two configurations are both path-dependent.

Element	W_D^* (MJ)	E_A^* (%)	E_A^{**} (%)	E_D(%)	Type of elasticity
C	40.6	8.3E–5	2.1E–14	–8.3E–5	Hyper
AB	36.8	0.393	0.011	–3.18	HYPO
AD	38.9	1.1E–5	–1.0E–8	–1.1E–5	Hyper
AN	36.8	0.393	0.011	–3.18	HYPO
F	41.3	8.6E–5	–2.6E–15	–8.6E–5	Hyper

Table 11.1 Path-independence tests. Errors in the work and description of the type of elastic response.

Table 11.1 presents the results for the Cosserat point element (C) and for the other enhanced strain/incompatible mode elements. The theoretical values of $\{E_A^*, E_A^{**}, E_D\}$ for the Cosserat point element are zero. Consequently, the numerical values for the Cosserat solution in Table 11.1 represent the combined numerical error due to: the convergence criterion used to satisfy equilibrium, machine precision and numerical integration of the work done using the trapezoidal rule. Thus, the error in the constitutive equation of a particular element can be determined by comparing the relative error with that of the Cosserat element. Furthermore, it is noted that the differences in the values of the work W_D^* given in Table 11.1 reflect differences in the specific treatment of inhomogeneous deformations in each of the elements. Moreover, the errors E_A^{**} associated with a cycle composed of a path and its reverse path are typically smaller than those E_A^* associated with a general cycle. The errors E_D associated with two different paths to the same point can be up to 10 times those of E_A^*. Also, it is noted that negative values of E_A^* or E_A^{**} in Table 11.1 indicate that the element generates energy whereas positive values of these quantities indicate that the element dissipates energy.

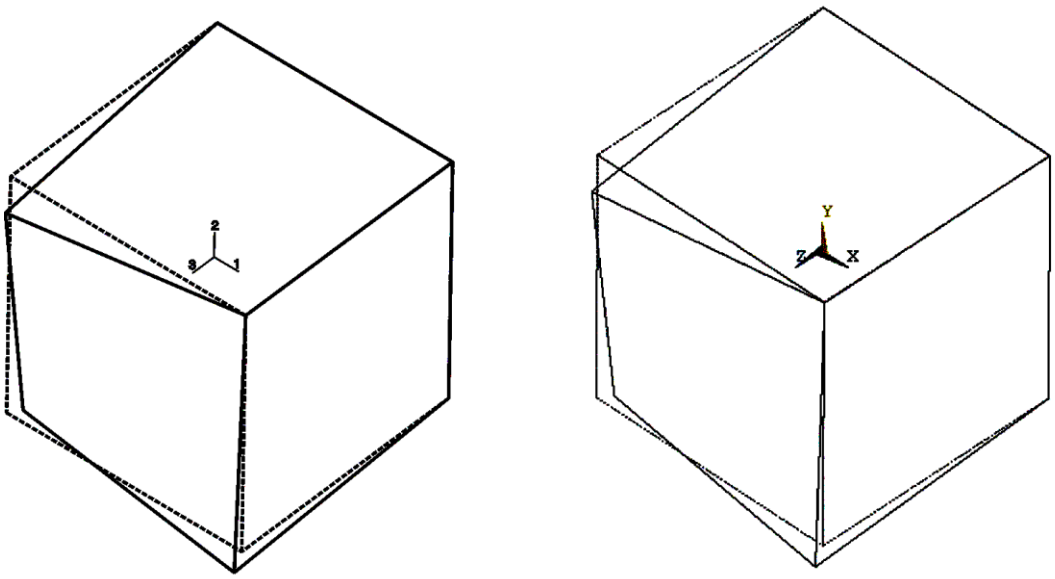

(a) AB (b) AN

Fig. 11.2 Residual element distortion after 10 deformation cycles ABCDEFA for the inelastic elements (AB) and (AN). The displacements have not been enhanced.

The results in Table 11.1 indicate that the elements (AD) and (F) exhibit hyperelastic response for the paths considered, while the elements (AB) and (AN) exhibit hypoelastic response. Although the values of E_A^* in Table 11.1 for the elements (AB) and (AN), based on incompatible modes or enhanced strains, seem relatively small, these errors are cumulative when multiple cycles are performed. Figure 11.2 shows the residual element distortion after 10 deformation cycles ABCDEFA. It is emphasized that the displacements in Fig. 11.2 have not been enhanced. Also, it is noted that multiple deformation cycles need to be calculated for problems like rolling tires or vibrating MEMS devices so that these accumulated errors may be quite significant in certain calculations.

12. Example problems of thin structures with irregular element shapes

The deformation field associated with the solution of a practical problem typically is inhomogeneous so that the response of the CPE is influenced by the specific form of the inhomogeneous strain energy being used. Mesh refinement tends to cause the response of the CPE to be dominated by its response to homogeneous deformations with the influence of the inhomogeneous strain energy becoming negligible. Consequently, since the CPE satisfies the patch test the predictions of the CPE should converge to the exact solution with mesh refinement. However, the rate of convergence is influenced by details of the functional form for the inhomogeneous strain energy.

In order to study the accuracy of the inhomogeneous strain energy function it is best to focus attention on problems that are dominated by inhomogeneous deformations. This can be accomplished by focusing on the response of thin structures to bending fields. More details of the examples discussed in this section can be found in (Jabareen and Rubin, 2007a,b,e).

12.1: Shear load on a thin cantilever beam (small deformations)

Figure 12.1 shows a sketch of a thin cantilever beam with dimensions

$$L = 200 \text{ mm} , \quad H = W = 10 \text{ mm} , \tag{12.1}$$

which is fully clamped at one of its ends and is subjected to a shear force P (modeled by a uniform shear stress) applied in the $\mathbf{e}_2$ direction to its other end. The lateral surfaces are traction free. The mesh {20n×n×n} is defined by distorting the middle cross-section in its reference configuration (using the parameters a_1,a_2,a_3,a_4 shown in Fig. 12.1), with 10n elements on each side of this cross-section and n elements in each of the $\mathbf{e}_2$ and $\mathbf{e}_3$ directions.

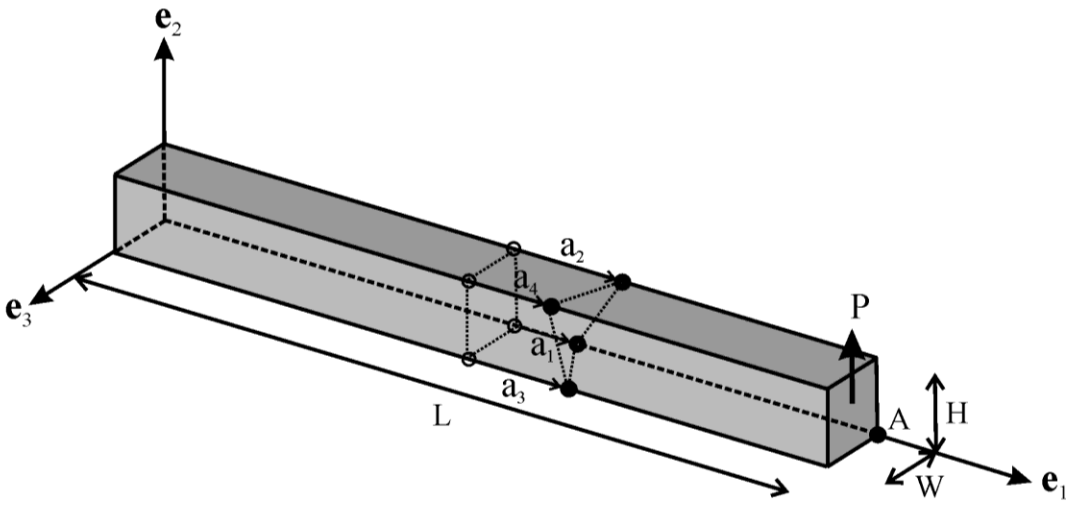

Fig. 12.1 Shear load on a thin cantilever beam. The irregular element mesh is based on the distorted center cross-section.

Two cases of element irregularity are considered

$$\text{Case I: } a_1 = a\ ,\ a_2 = -a\ ,\ a_3 = a\ ,\ a_4 = -a\ ,$$

$$\text{Case II: } a_1 = a\ ,\ a_2 = a\ ,\ a_3 = -a\ ,\ a_4 = -a\ , \tag{12.2}$$

where the parameter a/H defines the element irregularity. Both of these cases cause the middle surface to remain planar with the normal to that surface being in the $\mathbf{e}_1$–$\mathbf{e}_2$ plane for Case I and being in the $\mathbf{e}_1$–$\mathbf{e}_3$ plane for Case II. The value

$$u^*_{A2} = 0.21322 \text{ mm} \quad \text{for} \quad P = 0.1 \text{ N} \tag{12.3}$$

of the $\mathbf{e}_2$ component of the displacement of point A (see Fig. 12.1) predicted by the generalized CPE (C) with the most refined mesh (n=5) and zero irregularity (a/H=0) is considered to be exact and the error E associated with the predictions u_{A2} of other calculations for the same value of P is defined by

$$E = \frac{u_{A2} - u^*_{A2}}{|u^*_{A2}|} \quad . \tag{12.4}$$

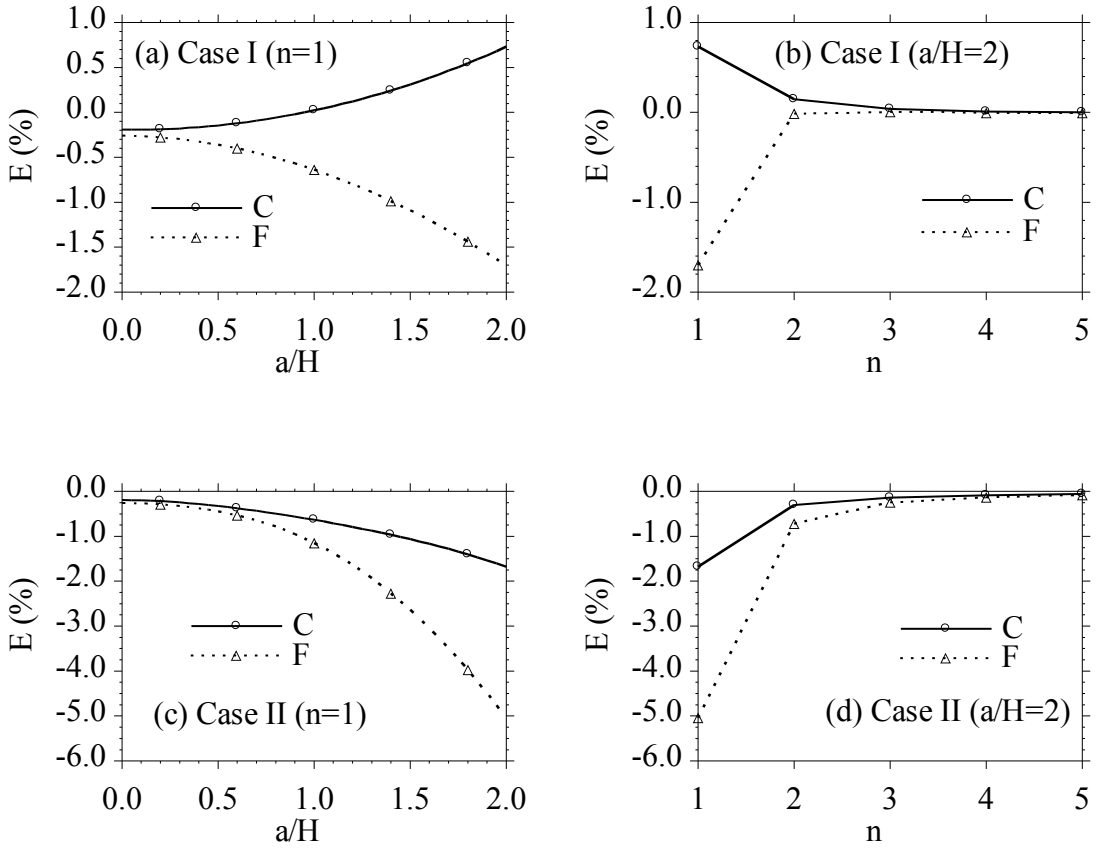

Fig. 12.2 Shear load on a thin cantilever beam (small deformations). (a,c) Errors in the displacement of the point A in the $\mathbf{e}_2$ direction versus the distortion parameter a/H and; (b,d) the errors versus n for the mesh {20n×n×n} defined for two cases of element distortion.

Figures 12.2a,b show the results for Case I and Figs. 12.2c,d show the results for Case II. The error is plotted as a function of the irregularity parameter a/H in Figs. 12.2a,c and convergence is examined in Figs. 12.2b,d. Ideally the response should be insensitive to the value of a/H. These figures show that the two elements converge to the same value

for the refined mesh (n=5) and large irregularity a/H=2. They also show that the predictions of (C) are slightly more accurate than those of (F).

12.2: Shear load on a thin slanted cantilever beam (small deformations)

Figure 12.3 shows a sketch of a thin slanted cantilever beam with dimensions (12.1) and with the slanting angle θ. The boundary conditions are the same as those for the previous example except that the shear load P is applied in the $\mathbf{e}_3$ direction to cause out-of-plane bending. Again the mesh is taken to be {20n×n×n} with 20n elements in axial direction of the beam. All of the elements have parallelogram cross-sections in the $\mathbf{e}_1$–$\mathbf{e}_2$ plane with sides parallel to the ends of the beam.

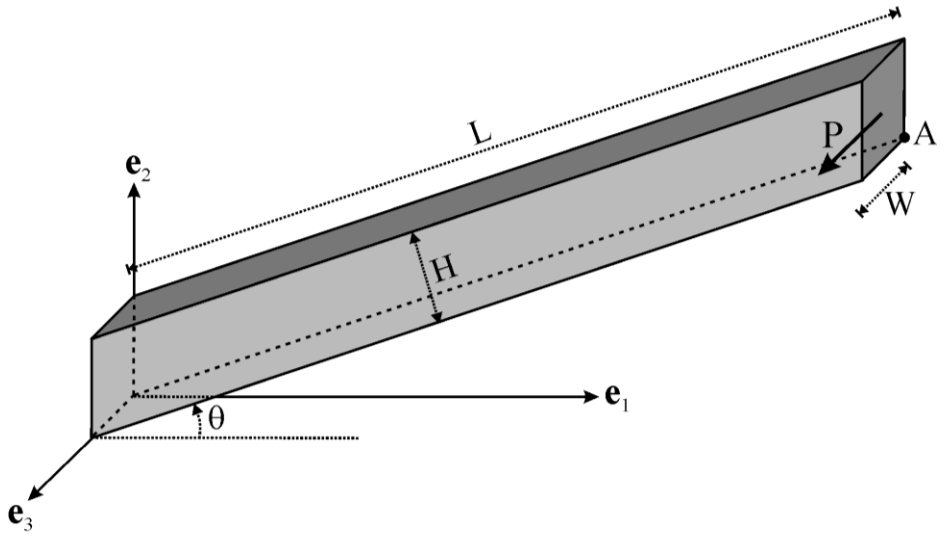

Fig. 12.3 Shear load on a thin slanted cantilever beam.

Figure 12.4a shows the displacement component u_{A3} of point A (see Fig. 12.3) in the $\mathbf{e}_3$ direction as a function of θ for the most refined mesh (n=5). The error E in u_{A3} is defined in a similar manner to (12.4) with the exact value u^*_{A3} taken to be that predicted by (C) for each value of θ with n=5 and with the load P given by (12.3). Figures 12.4b,c

show that (C) and (F) converge to the same values and that (C) is slightly more accurate than (F) for n=1 and large values of θ.

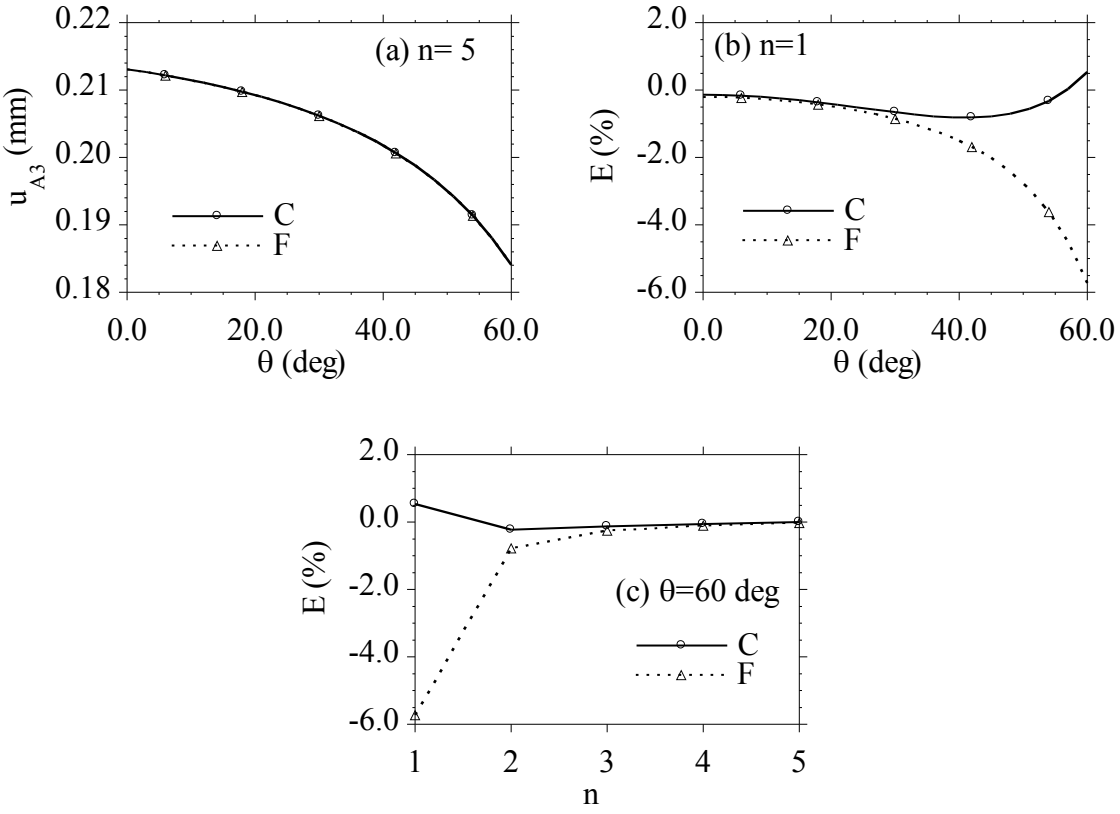

Fig. 12.4 Shear load on a thin slanted cantilever beam (small deformations). (a) Displacement u_{A3} of the point A in the $\mathbf{e}_3$ direction versus the angle θ for n=5 with the mesh {20n×n×n}; (b) errors in u_{A3} versus θ for n=1; (c) errors in u_{A3} versus n for θ=60 deg.

12.3: Lateral torsional buckling of a thin cantilever beam (large deformations)

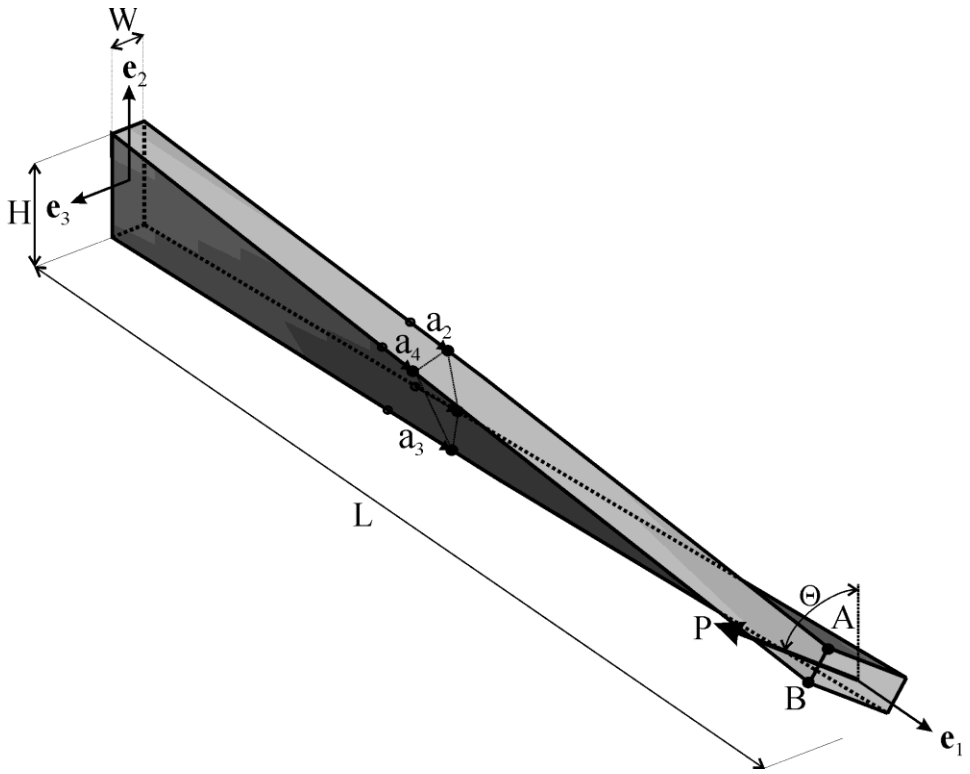

Fig. 12.5 Shear load on a thin twisted cantilever beam. The element mesh is based on the distorted center cross-section.

Figure 12.5 shows a sketch of a thin twisted cantilever beam which in its unstressed reference configuration has length L and a rectangular cross-section with height H and width W given by

$$L = 200 \text{ mm} , \quad H = 10 \text{ mm} , \quad W = 2 \text{ mm} \quad . \tag{12.5}$$

Each of the cross-sections is twisted by the angle θ which varies linearly from zero at the clamped end to Θ at the loaded end. Also, the load P is applied in the constant direction parallel to the long edges of the rectangular cross-section in its reference configuration. In order to stimulate lateral torsional buckling the value of Θ is taken to 0.1 deg which introduces a small imperfection in the reference geometry of the beam. Furthermore, the

element irregularity shown in Fig. 12.5 is specified by Case I in (12.2) and the mesh is given by {20n×n×n} with 20n elements in axial direction of the beam.

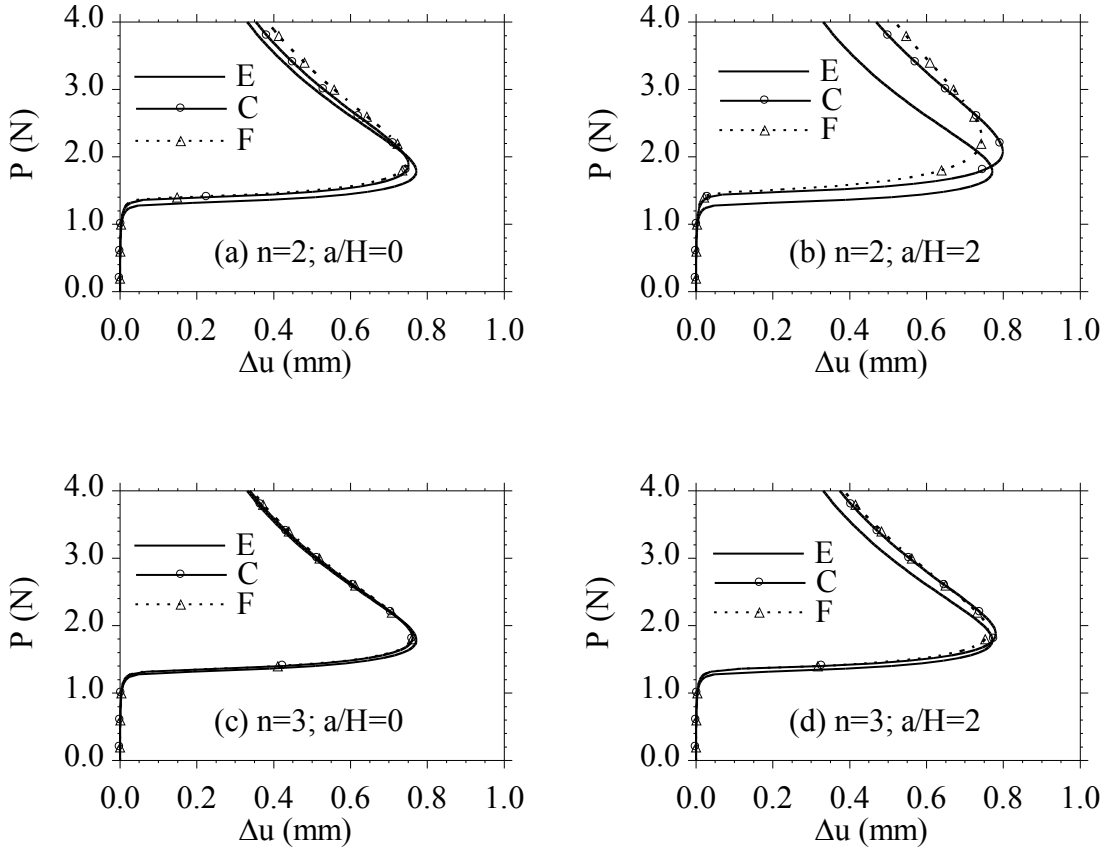

Fig. 12.6 Large deformation lateral torsional buckling of a thin cantilever beam with a small pre-twist Θ=0.1 deg. using the mesh {20n×n×n}. The influence of element irregularity is shown in Figs. 12.6a,b for n=2 and in Figs. 12.6c,d for n=3.

To investigate rotation of the beam's end it is convenient to consider the difference in the displacements of the points A and B shown in Fig. 12.5. Specifically, the quantity Δu is defined by

$$\Delta u = (\mathbf{u}_B - \mathbf{u}_A) \bullet \mathbf{e}_2 \quad . \tag{12.6}$$

Figure 12.6 shows the results for large deformation lateral torsional buckling of a thin cantilever beam. In this figure the curves denoted by (E) are predicted by (C) with n=5 and a/H=0 and are considered to be exact. The results in this figure show that for n=2 the predictions are not yet converged and are sensitive to element irregularity whereas for n=3 the predictions are reasonably converged and reasonably insensitive to element irregularity. Also, it can be seen that (C) and (F) converge to the same results.

12.4: Point load on the center of a thin fully clamped rhombic plate (small deformations)

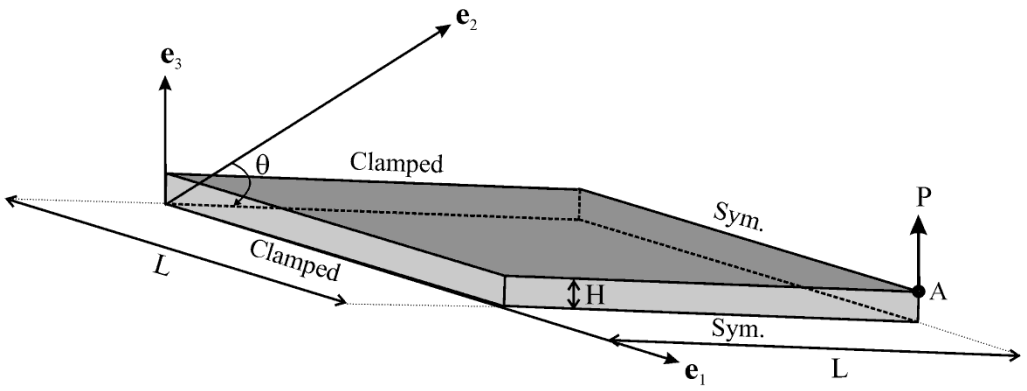

Fig. 12.7 Point load on the center of a thin fully clamped rhombic plate.

Figure 12.7 shows a sketch of one quarter of a thin fully clamped rhombic plate with dimensions

$$L = 500 \text{ mm} , \quad H = 10 \text{ mm} , \tag{12.7}$$

which is loaded at its center by a point force. The value L corresponds to one half of the actual length of each edge and the value

$$P = 1 \text{ N} , \tag{12.8}$$

corresponds to one quarter of the load that would be applied to the center of the entire plate. The mesh used for the quarter region of the plate is defined by {10n×10n×n} with n elements through the thickness.

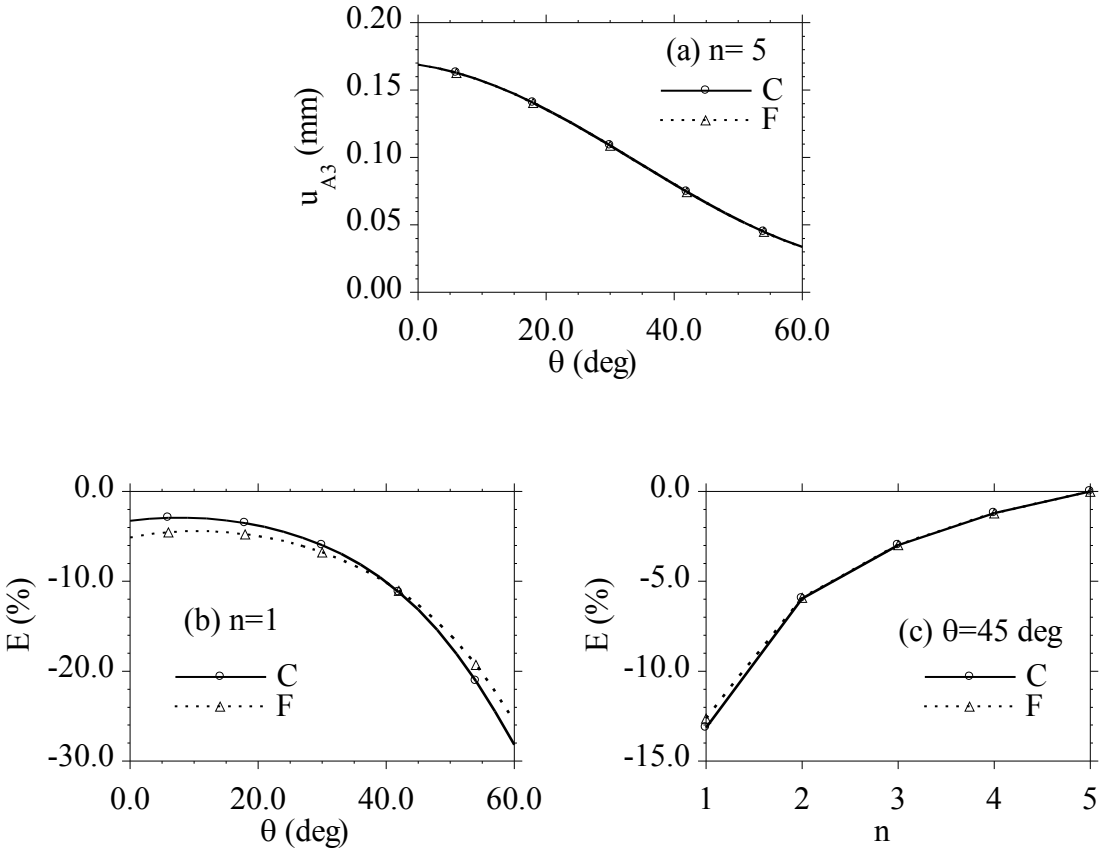

Fig. 12.8 Point load on the center of a thin fully clamped rhombic plate (small deformations). Displacement u_{A3} of the point A in the $\mathbf{e}_3$ direction versus the angle θ for n=5 with the mesh {10n×10n×n}; (b) errors in u_{A3} versus θ for n=1; (c) errors in u_{A3} versus n for θ=45 deg.

Figure 12.8a shows the component u_{A3} of the displacement of the point A in the $\mathbf{e}_3$ direction as a function of θ for the most refined mesh (n=5). The error E in this displacement is defined in a similar manner to (12.4) with the exact value u^*_{A3} taken to be

that predicted by (C) for each value of θ with n=5 and the load P given by (12.8). Also, Figs. 12.8b,c show that (C) and (F) converge to the same values.

12.5: Point load on the center of a thin fully clamped square plate with an irregular element mesh (small deformations)

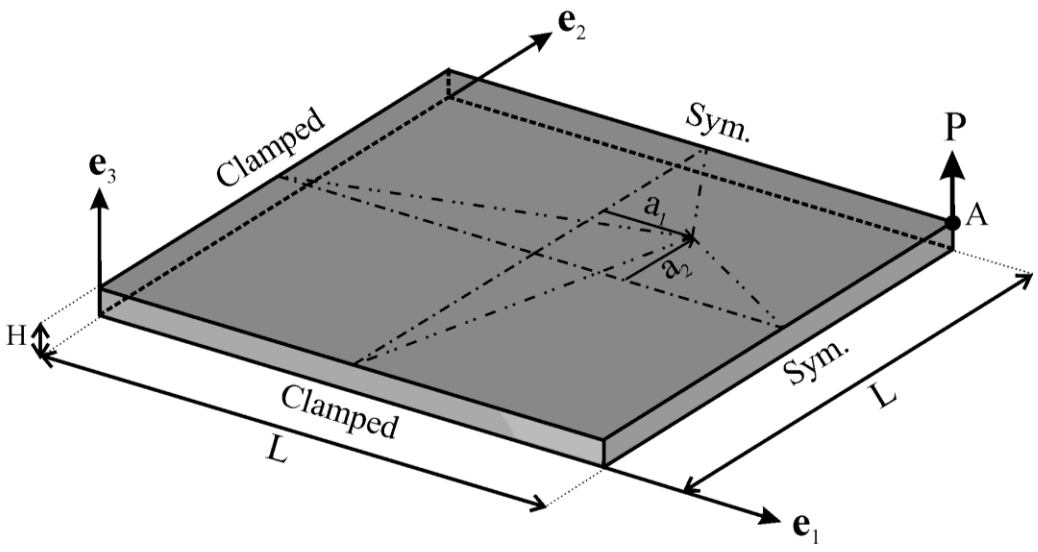

Fig. 12.9 Point load on the center of a thin fully clamped square plate with an irregular element mesh.

Figure 12.9 shows a sketch of one quarter of a thin fully clamped square plate with dimensions (12.7) that is loaded by a point force at its center. Only one quarter of the plate is modeled and the value P given by (12.8) corresponds to one quarter of the load that would be applied to the center of the entire plate. Irregular elements are specified by moving the center point of the quarter section to the position characterized by the lengths a_1 and a_2 (shown in Fig. 12.9) defined by two cases

$$\text{Case I: } a_1 = a_2 = a \ , \ -1 \le \frac{4a}{L} \le 1 \ ,$$

$$\text{Case II: } a_1 = \frac{L}{4}\cos(\theta)\ ,\ a_2 = \frac{L}{4}\sin(\theta)\ \ ,\ 0 \le \theta \le 2\pi\ \ . \tag{12.9}$$

The quarter section of the plate is meshed by {10n×10n×n} with each subsection being meshed by {5n×5n×n} and with n elements through the thickness. The error E in the displacement component u_{A3} of point A in the $\mathbf{e}_3$ direction is defined in a similar manner to (12.4) with the exact value u^*_{A3} taken to be that predicted by (C) for regular elements (a/L=0) with n=5

$$u^*_{A3} = 0.16893 \text{ mm} \ \text{ for } \ P = 1 \text{ N}\ \ . \tag{12.10}$$

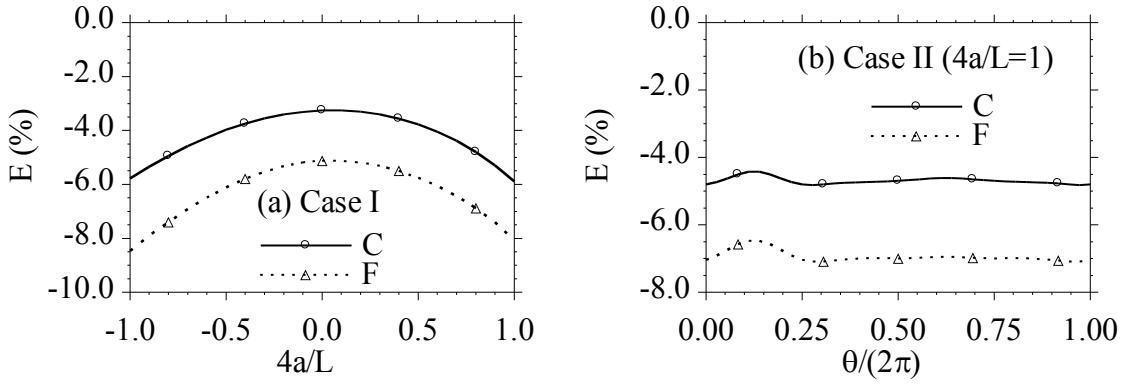

Fig. 12.10 Point load on the center of a thin fully clamped square plate (small deformations). Errors in the displacement of the point A in the $\mathbf{e}_3$ direction versus the distortion parameters (a) 4a/L and; (b) the angle θ for two cases of element irregularity with the mesh {10×10×1}.

Figures 12.10a,b show the error for n=1 as a function of the irregularity parameter 4a/L for Case I (Fig. 12.10a) and as a function of θ/(2π) for Case II (Fig. 12.10b). From these figures it can be seen that that (C) and (F) are both relatively insensitive to the magnitude and type of element irregularity.

12.6: Point load on the corner of a thin partially clamped rhombic plate (large deformations)

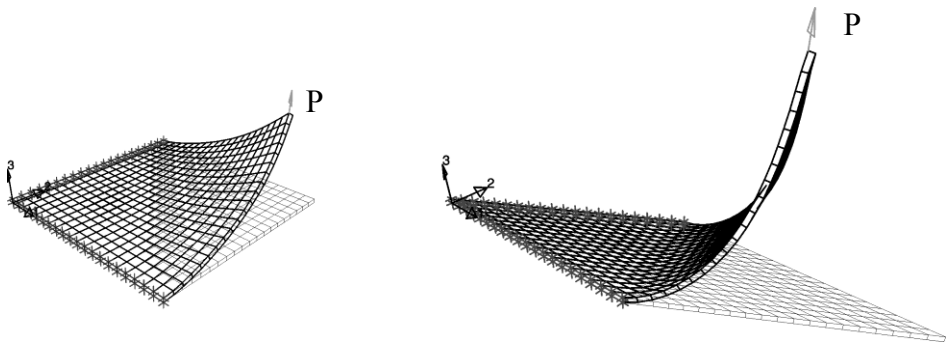

(a) θ = 0 deg (b) θ = 60 deg

Fig. 12.11 Point load on a partially clamped rhombic plate (large deformations).

Predictions of the generalized CPE for the mesh {10n×10n×1} with n = 2 and P = 1 kN.

Figure 12.11 shows the deformed shapes of a thin partially clamped rhombic plate subjected to a point load on its corner for two different angles θ and the same value of the load P. The plate is fully clamped on two edges and the other edges and major surfaces are traction free. The dimensions are given by (4.8) as shown in Fig. 11 (with L now being the length of the plate's edge) and the point force P given by

$$P = 1 \text{ kN} \ . \tag{12.11}$$

The mesh is specified by {10n×10n×1} and the exact values u_3^* of the displacement of the corner in the $\mathbf{e}_3$ direction is determined by the most refined solution (C) with n=5

$$u_3^* = 0.21084 \text{ m} \ \text{ for } \theta = 0 \text{ deg} \ , \quad u_3^* = 0.39306 \text{ m} \ \text{ for } \theta = 60 \text{ deg} \ . \tag{12.12}$$

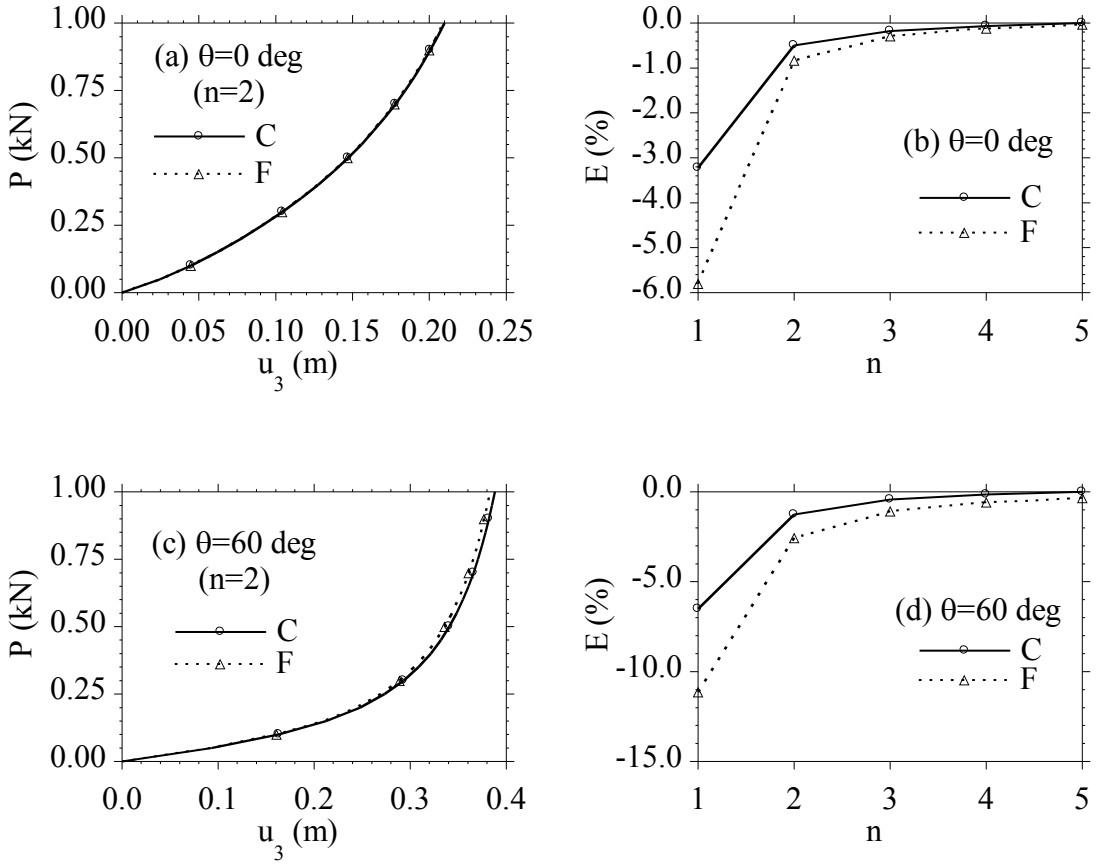

Fig. 12.12 Point load on a partially clamped rhombic plate (large deformations). Predictions of the load P versus displacement u_3 at the loaded corner and convergence of the error in the displacement for the mesh {10n×10n×1} with the load P = 1 kN and different angles θ.

Figures 12.12 show the load P versus displacement curves for n=2 and the convergence curves for two values of the angle θ. Comparison of Figs. 12.12a,c shows that the rhombic plate with angle θ=60 deg is more flexible than that for θ=0 deg and that (C) and (F) converge to the same solution. Also, Fig. 12.12d shows that the convergence properties of (C) are slightly better than those of (F) for the case when θ=60 deg.

13. Example problems exhibiting robustness to hourglass instabilities

Reese and Wriggers (1996, 2000) have shown that enhanced strain formulations, like that proposed by Simo et. al. (1993), can predict unphysical hourglass buckling modes for plane strain compression of a block. In order to examine this phenomena (Jabareen and Rubin, 2007a) considered a square block with edge length L=1 m which is compressed between two smooth rigid parallel end plates with the other two edges being free (see Fig. 13.1. Plane strain deformations are modeled using one 3-D element through the block's thickness and eliminating displacements in the out-of-plane direction.

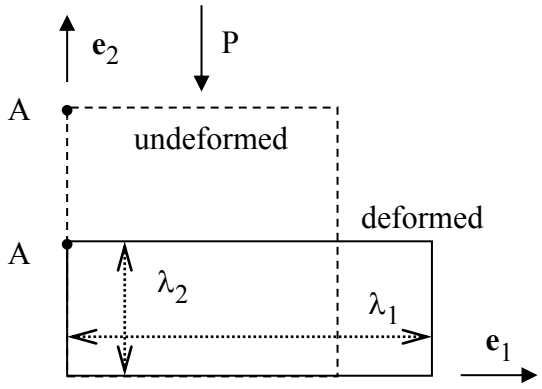

Fig. 13.1 Plane strain compression of a block showing the load P and the stretches λ_1 and λ_2 for the homogeneous solution.

For the homogeneous solution the stretches in the $\mathbf{e}_1$ and $\mathbf{e}_2$ directions are denoted by λ_1 and λ_2, respectively (see Fig. 13.1). At a critical value of λ_2 (< 1) the block buckles in its plane. In order to calculate the post-buckling response of this structure it is necessary to use special methods like arc-length control because a spring-back phenomena occurs

as the block buckles in shear. Moreover, a small imperfection is introduced in the reference mesh to trigger the shear buckling mode. Figure 13.2 shows that (C) predicts physical shear buckling modes for two nearly perfect regular meshes {10×10×1} and {20×20×1} and for two nearly perfect irregular meshes. From this figure it can be seen that the effect of element irregularity is not large.

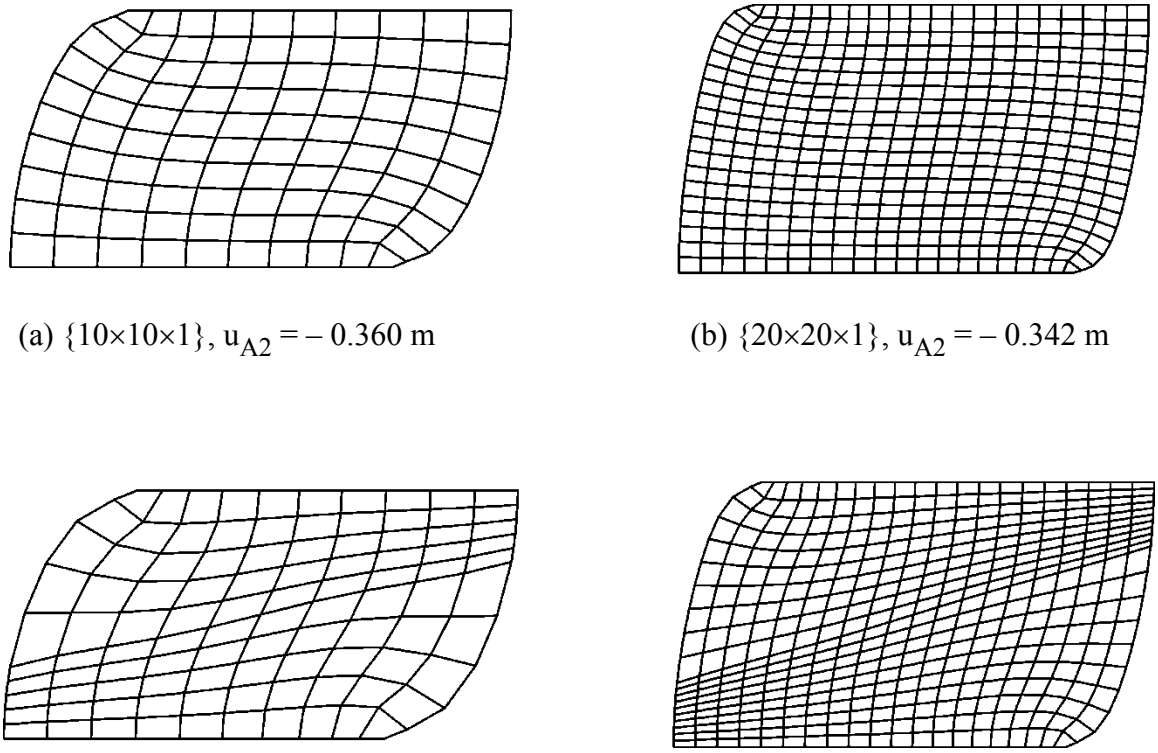

(a) {10×10×1}, $u_{A2} = -0.360$ m

(b) {20×20×1}, $u_{A2} = -0.342$ m

(c) {10×10×1}, $u_{A2} = -0.389$ m

(d) {20×20×1}, $u_{A2} = -0.348$ m

Fig. 13.2 Compression of a block. Physical shear buckling modes predicted by (C) for: (a,b) two nearly perfect regular meshes {10×10×1} and {20×20×1}; and (c,d) two nearly perfect irregular meshes.

Fig. 13.3 shows the predictions of an element in ABAQUS (AB) which is based on reduced integration with hourglass control. From this figure it can be seen that this element (AB) produces physical shear buckling which follows the predictions of the

Cosserat element (C). However, (AB) ceases to converge and thus cannot predict the full post-buckling behavior. Moreover, it is noted that the buckled mode predicted by (AB) shown in Fig. 13.3 is presented for the load just before the program ceased to converge.

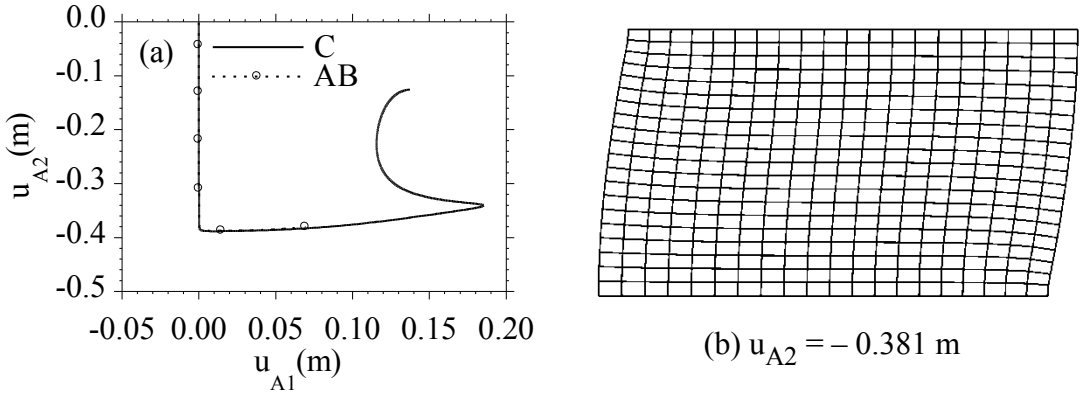

(b) $u_{A2} = -0.381$ m

Fig. 13.3 Compression of a block. Predictions of (C) and (AB) in ABAQUS for a nearly perfect regular mesh {20×20×1}; (a) displacement components; (b) compressive force P; and (b) post-buckling shape.

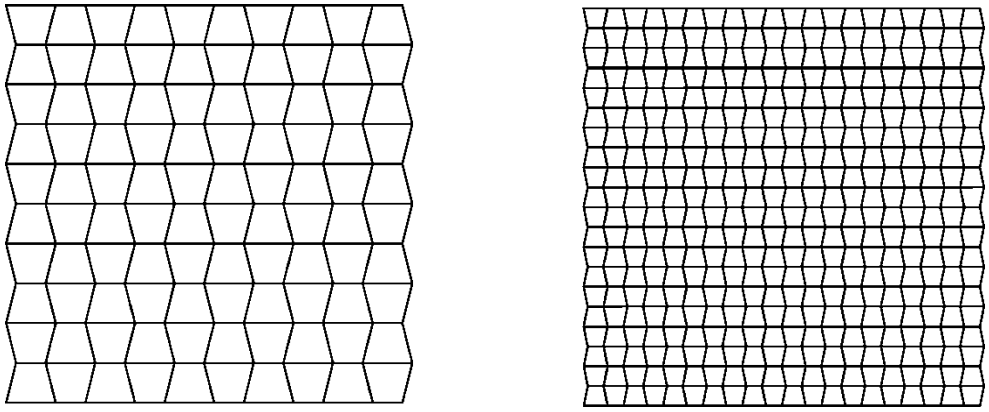

(a) {10×10×1}, $u_{A2} = -0.330$ m (b) {20×20×1}, $u_{A2} = -0.330$ m

Fig. 13.4 Compression of a block. Unphysical hourglass buckling modes at bifurcation predicted by (F) for two perfect regular meshes {10×10×1} and {20×20×1}.

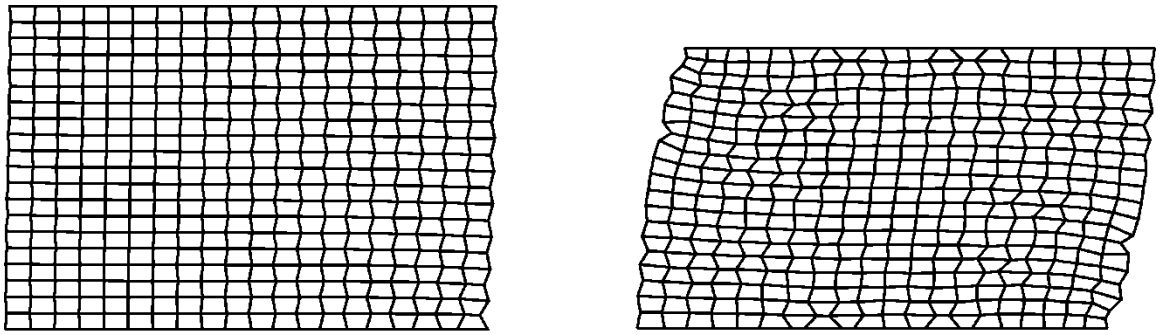

(a) (AB), $u_{A2} = -0.297$ m

(b) (AD), $u_{A2} = -0.389$ m

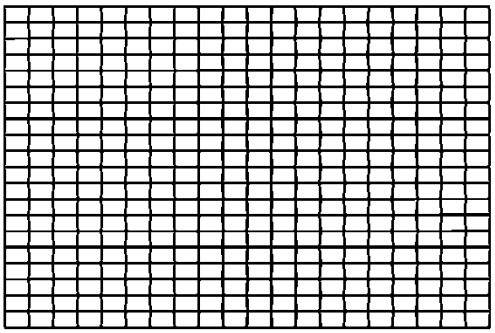

(c) (AN), $u_{A2} = -0.295$ m

Fig. 13.5 Compression of a block. Unphysical hourglass buckling modes predicted by (AB), (AD) and (AN) for a refined nearly perfect regular mesh {20×20×1}.

As mentioned previously, the elements based on enhanced strains and incompatible modes can exhibit unphysical hourglass modes for problems with high compression combined with bending. Specifically, Fig. 13.4 shows the results of calculations using the enhanced strain element in FEAP (F) for two perfect regular meshes {10×10×1} and {20×20×1}. From this figure it can be seen that at the bifurcation point $u_{A2} = -0.330$ m (the point where the lowest eigenvalue of the global tangent stiffness changes sign

between $u_{A2} = -0.3303$ m and $u_{A2} = -0.3304$ m), the associated buckling mode shapes are characterized by unphysical hourglassing for both meshes.

The enhanced strain and incompatible mode elements in ABAQUS (AB), ADINA (AD) and ANSYS (AN) exhibit unphysical hourglasing that causes lack of convergence for (AB) and (AN). Figure 13.5 shows the deformed shapes predicted by these elements for a nearly perfect regular mesh {20×20×1} corresponding to the load just before the programs ABAQUS and ANSYS ceased to converge. The element (AD) predicts a post buckled response that is corrupted by hourglassing.

14. Example problems exhibiting robustness to near incompressibility

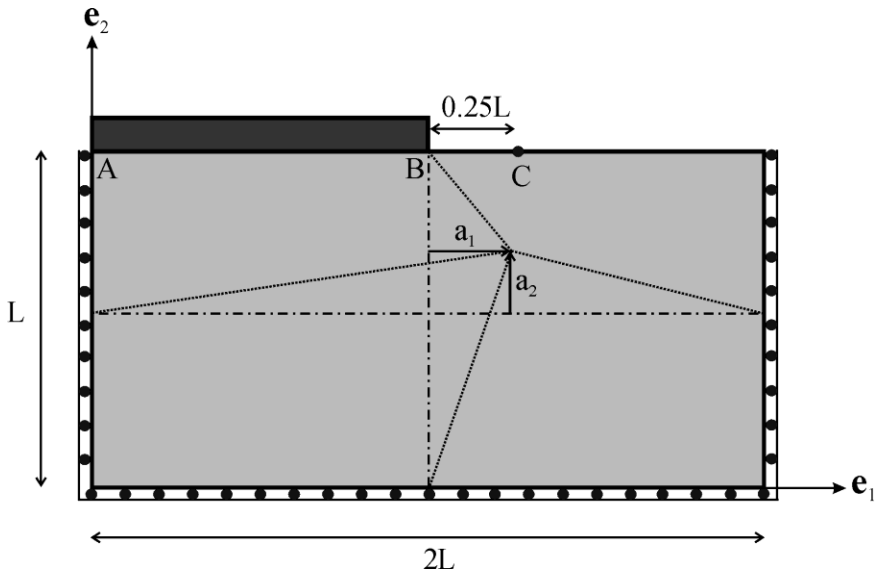

Fig. 14.1 Plane strain indentation of a rigid plate into a block showing the boundary conditions and definition of element irregularity.

Jabareen and Rubin (2007e) considered the example of plane strain indentation of a rigid plate into a nearly incompressible elastic block to examine the response of (C) in the nearly incompressible limit. Figure 14.1 shows a sketch of the boundary conditions on a block which has length 2L, height L and depth W. Material points on the block's sides and bottom remain in contact with a rigid container and are allowed to slide freely. The top surface of the block is loaded by a rigid plate (AB) of length L which makes perfect contact with the block so that material points in contact with the rigid plate move only vertically. The remaining half of the block's top surface is traction free and the dimensions of the block are given by

$$L = W = 1 \text{ m} \ . \tag{14.1}$$

Irregular meshes are defined by dividing the block into four subsections with the central node moving to the position characterized by the lengths $\{a_1, a_2\}$ (shown in Fig. 14.1) defined by two cases

$$\text{Case I: } a_1 = a\,,\ a_2 = 0\ ,\ -1 \le \frac{8a}{3L} \le 1\ ,\ u_{A2} = -0.1\ \text{m}\,,\ n = 5\,,$$

$$\text{Case II: } a_1 = 0\,,\ a_2 = a\ ,\ -1 \le \frac{8a}{3L} \le 1\ ,\ u_{A2} = -0.1\ \text{m}\,,\ n = 5\ . \qquad (14.2)$$

The entire block is meshed by $\{8n\times4n\times1\}$ with 4n elements in the $\mathbf{e}_1$ direction and 2n elements in the $\mathbf{e}_2$ in each of the subsections. The point C (shown in Fig. 14.1) is located on the free top surface at a distance 0.25 L from the corner B of the rigid plate. Also, the material is considered to be nearly incompressible.

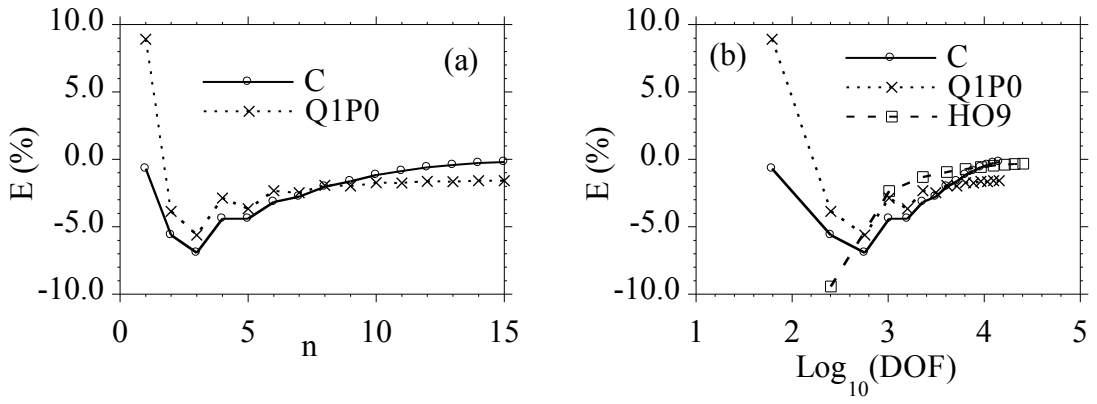

Fig. 14.2 Plane strain indentation of a rigid plate into a nearly incompressible block. Convergence of the error E in the displacement u_{C2} of the point C using the regular mesh $\{8n\times4n\times1\}$ for $u_{A2} = -0.1$ m versus: (a) n; and (b) versus the number of degrees of freedom DOF.

Figure 14.2 shows convergence of the solution for the regular (a=0) mesh {8n×4n×1} and $u_{A2} = -0.1$ m. The converged value u^*_{C2} of the displacement of the point C in the $\mathbf{e}_2$ direction predicted by (C) for a regular mesh with n=20 is considered to be exact and is given by

$$u^*_{C2} = 0.071895 \text{ m} \quad \text{for } u_{A2} = -0.1 \text{ m} \quad \text{with } n = 20 \quad . \tag{14.3}$$

The error E of in the values u_{C2} predicted by calculations of other elements and meshes is defined by an expression similar to (12.4). Figure 14.2 shows the convergence of this error predicted by {C, Q1P0, HO9}, where (HO9) denotes a mixed higher order nine node quadrilateral element in FEAP. This error is plotted relative to n for the mesh {8n×4n×1} in Fig. 14.2a and is plotted relative to the degrees of freedom (DOF, calculated for plane strain response) in Fig. 14.2b. From Fig. 14.2a it is not clear if (Q1P0) exhibits a locking behavior by converging to a value different from (C) or whether the convergence rate is very slow. To validate the converged value of (C) for n=20, calculations were also performed using the mixed higher order element (HO9) with the mesh {8n×4n×1} up to n=10. In particular, it can be seen in Fig. 14.2b that (HO9) tends to converge to the value predicted by (C).

Figure 14.3 presents the errors E in the displacement u_{C2} for two cases of element irregularity and for the mesh {8n×4n×1} with n=5 and $u_{A2} = -0.1$ m. Since there is a strain concentration near the edge of the plate it is expected that a non-fully converged solution will be sensitive to element irregularity. In particular, it can be seen from Fig. 14.3a that (Q1P0) is more sensitive to element irregularity than (C) for positive values of a for Case I which cause the elements near the plate's edge B to be more irregular. The

results in Fig. 14.3b show that the error reduces slightly for increasing positive values of a for Case II which cause the elements near the plate's edge B to be more refined.

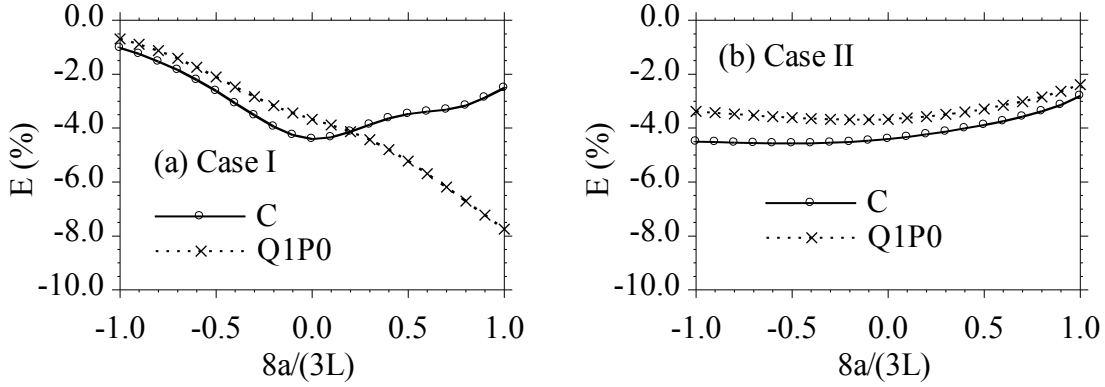

Fig. 14.3 Plane strain indentation of a rigid plate into a nearly incompressible block. Error E in the displacement u_{C2} of the point C for two cases of element irregularity and for the mesh {8n×4n×1} with n=5 and $u_{A2} = -0.1$ m.

Figure 14.4 shows nonlinear load curves using the regular mesh {8n×4n×1} for different values of n. These figures again show that (C) predicts more flexible response than (Q1P0) for the coarser meshes. Figure 14.5 shows the deformed shapes for the regular mesh {8n×4n×1} with n=3 for different values of loads. In particular, it can be seen that the flexibility of (C) allows the elements near the plate's corner to roll around the corner more easily than allowed by (Q1P0). Since the flexibility of (C) has been validated relative to the mixed higher order element (HO9) it is concluded that the stiffness shown by (Q1P0) is unphysical.

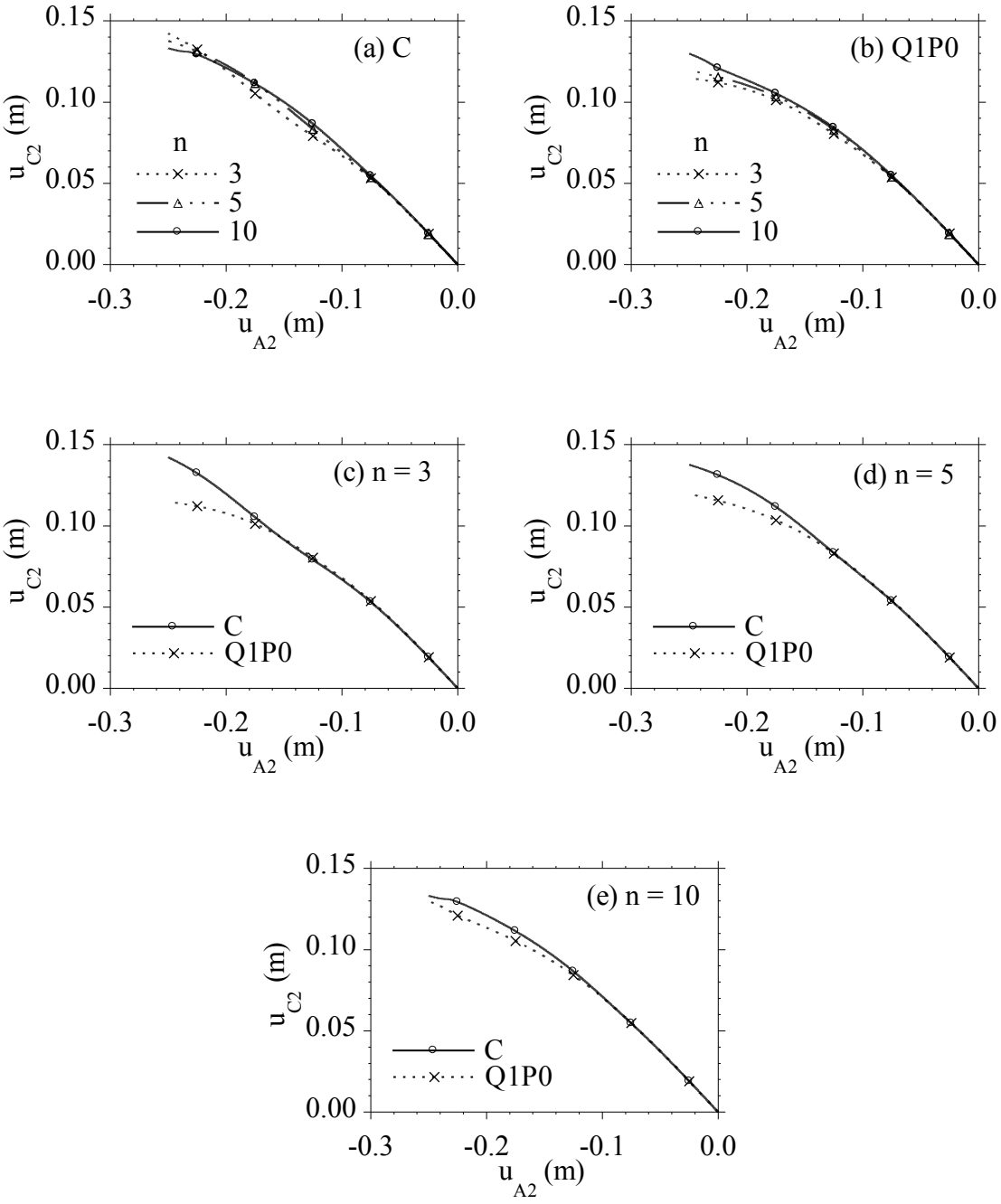

Fig. 14.4 Plane strain indentation of a rigid plate into a nearly incompressible block showing nonlinear load curves using the regular mesh {8n×4n×1} for different values of n.

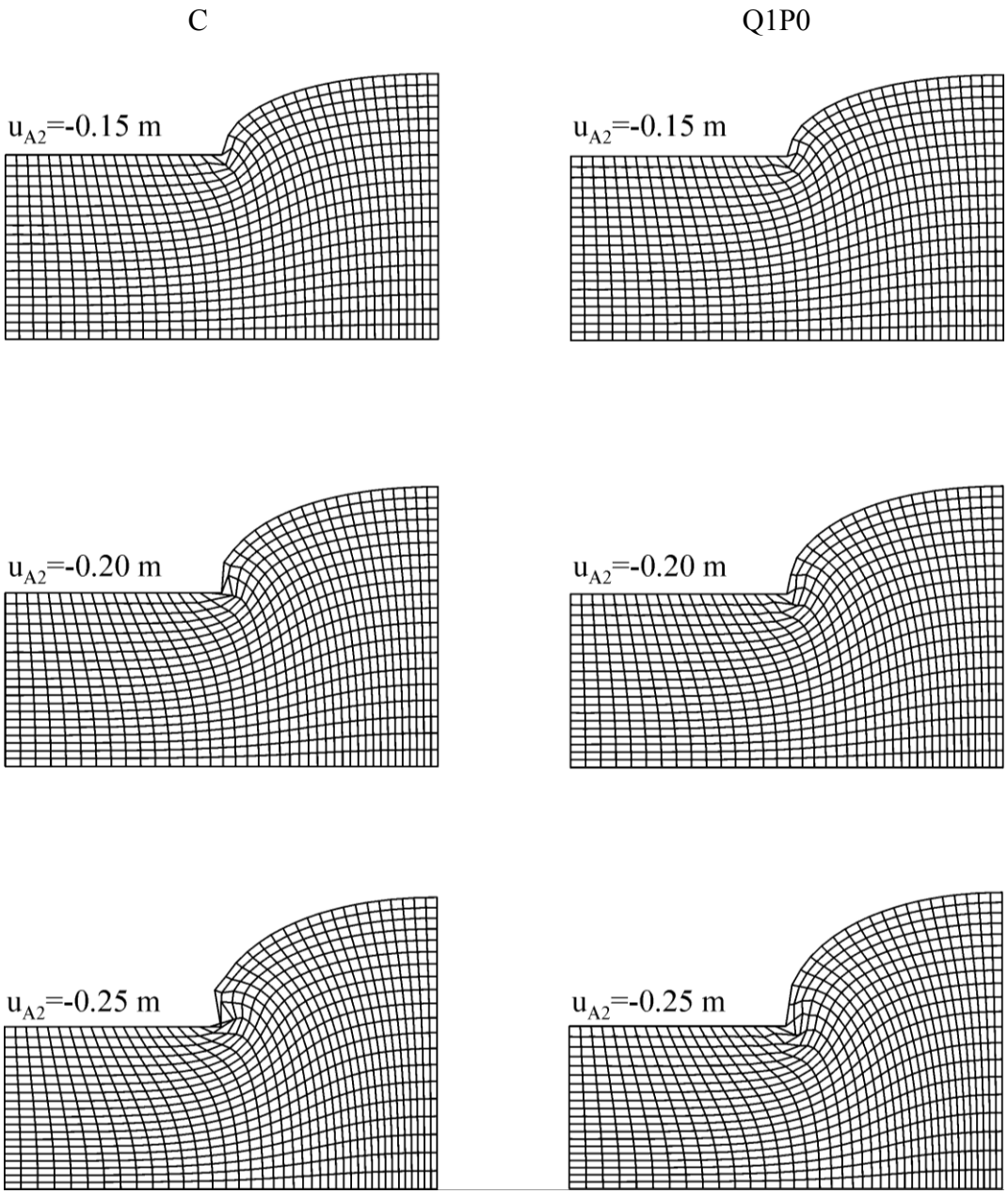

Fig. 14.5 Plane strain indentation of a rigid plate into a nearly incompressible block showing the deformed shapes for the regular mesh {8n×4n×1} with n=5. The left column shows the results for (C) and the right column shows the results (Q1P0).

15. Conclusions

The previous sections summarize the development of a 3-D brick Cosserat Point Element (CPE) for the numerical solution of problems in nonlinear elasticity. The CPE is based on the theory of a Cosserat point which is a continuum theory that introduces balance laws for the deformation of a structure that is "thin" in three-dimensions. In contrast with standard finite element methods, the CPE treats the finite element as a structure and the kinetic quantities are determined by derivatives of a strain energy that characterizes resistance to all modes of deformation of the structure. In particular, a nonlinear form of the patch test is used to place restrictions on this strain energy function which ensure that the CPE reproduces all homogeneous solutions exactly for all reference element shapes. Special attention has been focuses on developing an analytical form for the strain energy of inhomogeneous deformations that causes the predictions of the CPE to be relatively insensitive to element irregularity even for thin structures like shells and rods.

Example problems have been considered which show that the CPE is as accurate as elements based on enhanced strains and incompatible modes for thin structures and is free of the hourglass instabilities observed in these elements for deformations with high compression combined with bending. Also, the CPE is free of locking due to near incompressible material response. Consequently, the CPE is truly a user friendly element that can be used with confidence to solve problems in nonlinear elasticity.

Although the CPE approach has proved very successful for nonlinear elastic materials it is not clear how it can be generalized for more complicated material response. An elastic solid has the special simple property that it has a unique shape when it is

unloaded. In contrast, and elastic-viscoplastic material can have an infinite number of stress-free shapes which differ by a general homogeneous deformation. Thus, in order to generalize the CPE for elastic-viscoplastic materials it is necessary to first understand how the CPE can be generalized for fluids which have no unique stress-free shapes. At present it appears that this area of research will remain challenging for a number of years to come.

References

[1] ABAQUS Inc., Version 6.5-1, Providence RI 02909-2499.

[2] ADINA R & D Inc., Version 8.3.1, Watertown, MA 02472.

[3] ANSYS Inc., University Advanced Version 9, Canonsburg, PA 15317.

[4] Taylor RL (2005) FEAP - A Finite Element Analysis Program, Version 7.5, University of California, Berkeley.

[5] Belytschko T, Ong JSJ, Liu WK and Kennedy JM (1984) Hourglass control in linear and nonlinear problems. *Comp. Meth. Appl. Mech. Engrg.* 43:251-276.

[6] Boerner EFI, Loehnert S and Wriggers P. (2007) A new finite element based on the theory of a Cosserat point - extension to initially distorted elements for 2D plane strain. *Int. J. Numer. Meth. Engng*. 71: 454-472.

[7] Hutter R, Hora P and Niederer P (2000) Total hourglass control for hyperelastic materials. *Comp. Meth. Appl. Mech. Engrg.* 189:991-1010.

[8] Jabareen M, Rubin MB (2007a) Hyperelasticity and physical shear buckling of a block predicted by the Cosserat point element compared with inelasticity and hourglassing predicted by other element formulations. *Computational Mechanics*, 40:447-459.

[9] Jabareen M, Rubin MB (2007b) An improved 3-D Cosserat brick element for irregular shaped elements. *Computational Mechanics* 40:979–1004.

[10] Jabareen M, Rubin MB (2007c) Modified torsion coefficients for a 3-D brick Cosserat point element. *Computational Mechanics* 41: 517-525.

[11] Jabareen M, Rubin MB (2007d) A Cosserat point element (CPE) for nearly planar problems (including thickness changes) in nonlinear elasticity. Submitted to *International Journal for Engineering Science*.

[12] Jabareen M, Rubin MB (2007e) A generalized Cosserat point element (CPE) for isotropic nonlinear elastic materials including irregular 3-D brick and thin structures. Submitted to *Journal of Mechanics of Materials and Structure*.

[13] Loehnert S, Boerner EFI, Rubin MB and Wriggers P. (2005) Response of a nonlinear elastic general Cosserat brick element in simulations typically exhibiting locking and hourglassing. *Computational Mechanics* 36:255-265.

[14] Nadler B, and Rubin MB, (2003) A new 3-D finite element for nonlinear elasticity using the theory of a Cosserat point, *Int. J. Solids and Structures* 40: 4585-4614.

[15] Naghdi PM and Rubin, MB, (1995) Restrictions on nonlinear constitutive equations for elastic shells. *J. Elasticity* 39:133-163.

[16] Reese S and Wriggers P (1996) Finite element calculation of the stability behaviour of hyperelastic solids with the enhanced strain methods. *Zeitschrift fur angewandte Mathematik und Mechanik* 76:415-416.

[17] Reese S and Wriggers P. A stabilization technique to avoid hourglassing in finite elasticity. *Int. J. Numer. Meth. Engng.* 48:79-109, 2000.

[18] Reese S, Wriggers P and Reddy BD (2000) A new locking free brick element technique for large deformation problems in elasticity. Computers and Structures 75:291-304.

[19] Rubin MB (1985a) On the theory of a Cosserat point and its application to the numerical solution of continuum problems. *J. Appl. Mech.* 52:368-372.

[20] Rubin MB (1985b) On the numerical solution of one-dimensional continuum problems using the theory of a Cosserat point. *J. Appl. Mech.* 52:373-378.

[21] Rubin MB (1995) Numerical solution of two- and three-dimensional thermomechanical problems using the theory of a Cosserat point, *J. of Math. and Physics (ZAMP)* **46**, Special Issue, S308-S334. In *Theoretical, Experimental, And Numerical Contributions To The Mechanics Of Fluids And Solids*, Edited by J Casey and MJ Crochet, Brikhauser Verlag, Basel (1995).

[22] Rubin MB. (1996) Restrictions on nonlinear constitutive equations for elastic rods. *J. Elasticity* 44:9-36.

[23] Rubin MB (2000) *Cosserat Theories: Shells, Rods and Points*. Solid Mechanics and its Applications, Vol. 79, Kluwer, The Netherlands.

[24] Rubin MB. (2001) Numerical solution procedures for nonlinear elastic rods using the theory of a Cosserat point. *Int. J. Solids Structures* 38:4395-4437.

[25] Simo JC and Armero F (1992) Geometrically non-linear enhanced strain mixed methods and the method of incompatible modes. *Int. J. Numer. Meth. Engng.* 33:1413-1449.

[26] Simo JC, Rifai MS (1990) A class of mixed assumed strain methods and the method of incompatible modes. *Int. J. Numer. Meth. Engng.* 29:1595-1638.

[27] Simo JC, Armero F, Taylor RL (1993) Improved versions of assumed enhanced strain tri-linear elements for 3D finite deformation problems. *Comp. Meth. Appl. Mech. Engrg.* 110:359-386.

[28] Sokolnikoff IS (1956) *Mathematical Theory of Elasticity*. McGraw-Hill, New York.